



Intravenous nanoparticle vaccination generates stem-like TCF1⁺ neoantigen-specific CD8⁺ T cells

Faezzah Baharom¹, Ramiro A. Ramirez-Valdez¹, Kennedy K. S. Tobin¹, Hidehiro Yamane¹, Charles-Antoine Dutertre^{2,3,4}, Ahad Khalilnezhad^{2,5}, Glennys V. Reynoso⁶, Vincent L. Coble⁷, Geoffrey M. Lynn¹, Matthew P. Mulè^{8,9}, Andrew J. Martins⁸, John P. Finnigan¹⁰, Xiao Meng Zhang², Jessica A. Hamerman¹, Nina Bhardwaj¹⁰, John S. Tsang⁸, Heather D. Hickman¹, Florent Ginhoux¹, Andrew S. Ishizuka¹ and Robert A. Seder¹✉

Personalized cancer vaccines are a promising approach for inducing T cell immunity to tumor neoantigens. Using a self-assembling nanoparticle vaccine that links neoantigen peptides to a Toll-like receptor 7/8 agonist (SNP-7/8a), we show how the route and dose alter the magnitude and quality of neoantigen-specific CD8⁺ T cells. Intravenous vaccination (SNP-IV) induced a higher proportion of TCF1⁺PD-1⁺CD8⁺ T cells as compared to subcutaneous immunization (SNP-SC). Single-cell RNA sequencing showed that SNP-IV induced stem-like genes (*Tcf7*, *Slamf6*, *Xcl1*) whereas SNP-SC enriched for effector genes (*Gzmb*, *Klrg1*, *Cx3cr1*). Stem-like cells generated by SNP-IV proliferated and differentiated into effector cells upon checkpoint blockade, leading to superior antitumor response as compared to SNP-SC in a therapeutic model. The duration of antigen presentation by dendritic cells controlled the magnitude and quality of CD8⁺ T cells. These data demonstrate how to optimize antitumor immunity by modulating vaccine parameters for specific generation of effector or stem-like CD8⁺ T cells.

The clinical effectiveness of cancer immunotherapy, including checkpoint blockade and adoptive T cell therapy, is based on the magnitude, quality, breadth and ability of T cells to infiltrate tumors^{1–4}. Advances in rapid genomic sequencing has enabled the development of personalized cancer vaccines (PCVs) targeting tumor-specific mutations termed neoantigens. Early studies in mice^{5,6} and phase I clinical trials^{7–10} demonstrated the feasibility of PCVs to generate neoantigen T cell responses; however, the magnitude of CD8⁺ T cell responses has been limited to date¹⁰.

An important variable in improving CD8⁺ T cell responses with PCVs is the vaccine platform. Accordingly, we developed a self-assembling nanoparticle vaccine platform to standardize the delivery of long peptides (LPs)¹¹. At 20–50 nm in size, nanoparticles allow for efficient drainage via lymphatics and uptake by dendritic cells (DCs) that prime CD8⁺ T cells¹². Further, co-delivery of the antigen and Toll-like receptor 7/8 (TLR7/8) agonist (TLR7/8a) ensures DC maturation via TLR activation in the same cell that has acquired the antigen, to achieve optimal presentation to CD8⁺ T cells. Indeed, the SNP-7/8a vaccine platform generated higher magnitude and breadth of CD8⁺ T cells with antitumor efficacy when benchmarked against the most commonly used PCV approaches¹¹.

In addition to magnitude, the quality of CD8⁺ T cell responses can be an important determinant in protection against viral

infections and tumors^{13,14}. Studies elucidating the transcriptional and epigenetic heterogeneity of CD8⁺ T cells has provided important advances in understanding lineage differentiation, proliferative potential and functional capacity. In chronic lymphocytic choriomeningitis virus (LCMV) infection, T-cell specific transcription factor 1 (TCF1) was identified as a critical transcription factor that maintains a precursor population within the exhausted T cell (Tex) pool^{15–19}. Highly expressed in naive CD8⁺ T cells, TCF1 is downregulated during effector cell differentiation in response to pro-inflammatory cytokines such as interleukin-12 (IL-12) and type I interferons (IFNs)^{20,21}. Previously thought to be dysfunctional, a subset of PD-1⁺ Tex referred to as progenitor exhausted or stem-like cells that express TCF1 remain responsive to checkpoint inhibitors (CPIs); they maintain stem cell-like quality by retaining the capacity to proliferate and self-renew^{22–24}. Studies assessing CD8⁺ tumor-infiltrating lymphocytes (TILs) in humans identified gene signatures of stem-like cells including *Tcf7* (encoding TCF1), associated with better prognosis and response to checkpoint blockade^{25–30}. Adoptive transfer studies in mice showed that the self-renewing capacity of TILs was regulated by TCF1 (ref. ³¹) whereas cells lacking TCF1 were less effective in controlling tumor growth³². Collectively, these data suggest an important role for TCF1⁺PD-1⁺CD8⁺ T cells in mediating protection against viral infections and tumors.

¹Vaccine Research Center, National Institute of Allergy and Infectious Diseases, National Institutes of Health, Bethesda, MD, USA. ²Singapore Immunology Network, A*STAR, Singapore, Singapore. ³Program in Emerging Infectious Disease, Duke-National University of Singapore Medical School, Singapore, Singapore. ⁴Singhealth Translational Immunology and Inflammation Centre, Singapore, Singapore. ⁵Department of Microbiology and Immunology, Yong Loo Lin School of Medicine, National University of Singapore, Singapore, Singapore. ⁶Viral Immunity and Pathogenesis Unit, Laboratory of Clinical Immunology and Microbiology, National Institute of Allergy and Infectious Diseases, National Institutes of Health, Bethesda, MD, USA. ⁷Avidex Technologies, Baltimore, MD, USA. ⁸Systems Genomics and Bioinformatics Unit, Laboratory of Immune System Biology, National Institute of Allergy and Infectious Diseases, National Institutes of Health, Bethesda, MD, USA. ⁹Department of Medicine, University of Cambridge, Cambridge, UK. ¹⁰Department of Medicine, Division of Hematology/Oncology, Icahn School of Medicine at Mount Sinai, Tisch Cancer Institute, New York, NY, USA. ¹¹Immunology Program, Benaroya Research Institute, Seattle, WA, USA. ¹²Shanghai Institute of Immunology, Department of Immunology and Microbiology, Shanghai, China. ✉e-mail: rseder@nih.gov

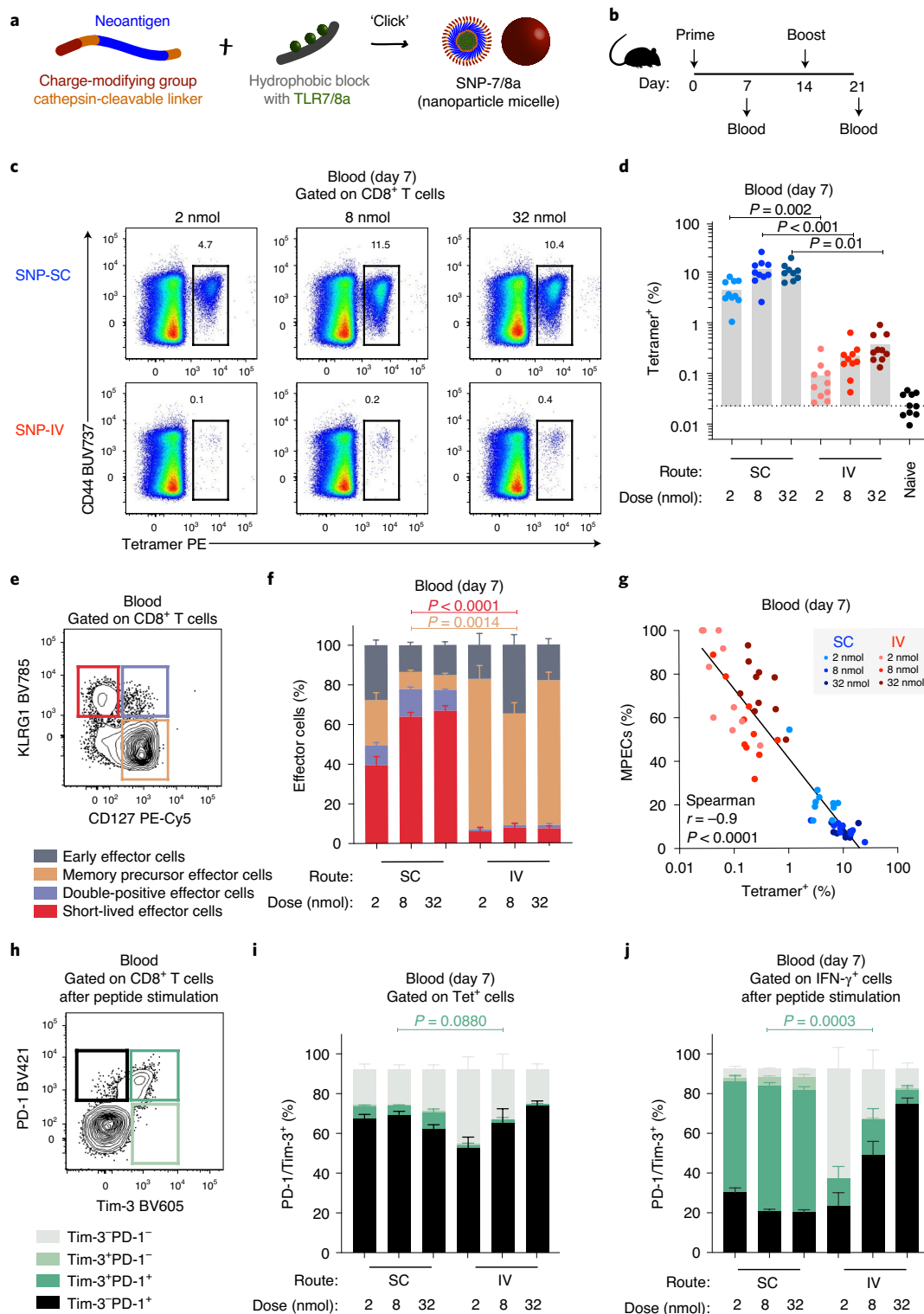


Fig. 1 | The route and dose of SNP-7/8a immunization controls the magnitude and phenotype of antigen-specific CD8 T cells. **a**, Schematic of peptide-TLR7/8 agonist vaccines that form self-assembling nanoparticles (SNP-7/8a). **b**, C57BL/6 mice ($n=10$) were vaccinated subcutaneously or intravenously at 2, 8 or 32 nmol on days 0 and 14 with SNP-7/8a containing Reps1, an MC38 neoantigen. Whole blood was collected on days 7 and 21 to measure the frequency of tetramer⁺ CD8⁺ T cells. **c**, Flow cytometric analysis of single cells stained with Reps1 tetramer and CD44 antibody. The numbers indicate the percentage of the cell population within the gate. **d**, Bar graphs summarizing the frequency of tetramer⁺ CD8⁺ T cells from blood ($n=10$) on day 7. **e**, CD8⁺ T cells were subdivided into MPECs (tan gate) or SLECs (crimson gate) based on CD127 and KLRG1 expression. **f**, Bar graphs showing the proportions of MPEC/SLEC subpopulations in blood on day 7 ($n=10$). **g**, The frequency of MPECs is negatively correlated with the frequency of tetramer⁺ CD8⁺ T cells. **h–j**, Tetramer⁺ cells can be subdivided into PD-1⁺ (black), Tim-3⁺ (light green) or PD-1⁺Tim-3⁺ (dark green) cells (**h**). The bar graphs show the proportions of PD-1/Tim-3 subpopulations on day 7 ($n=10$) for tetramer⁺ (**i**) and IFN-γ⁺ cells (**j**). Data are representative of two independent experiments. The bars represent the median. **d,f,i,j**, Statistics were assessed by Kruskal-Wallis test with Dunn's correction for multiple comparisons. **g**, Statistics were assessed by Spearman correlation.

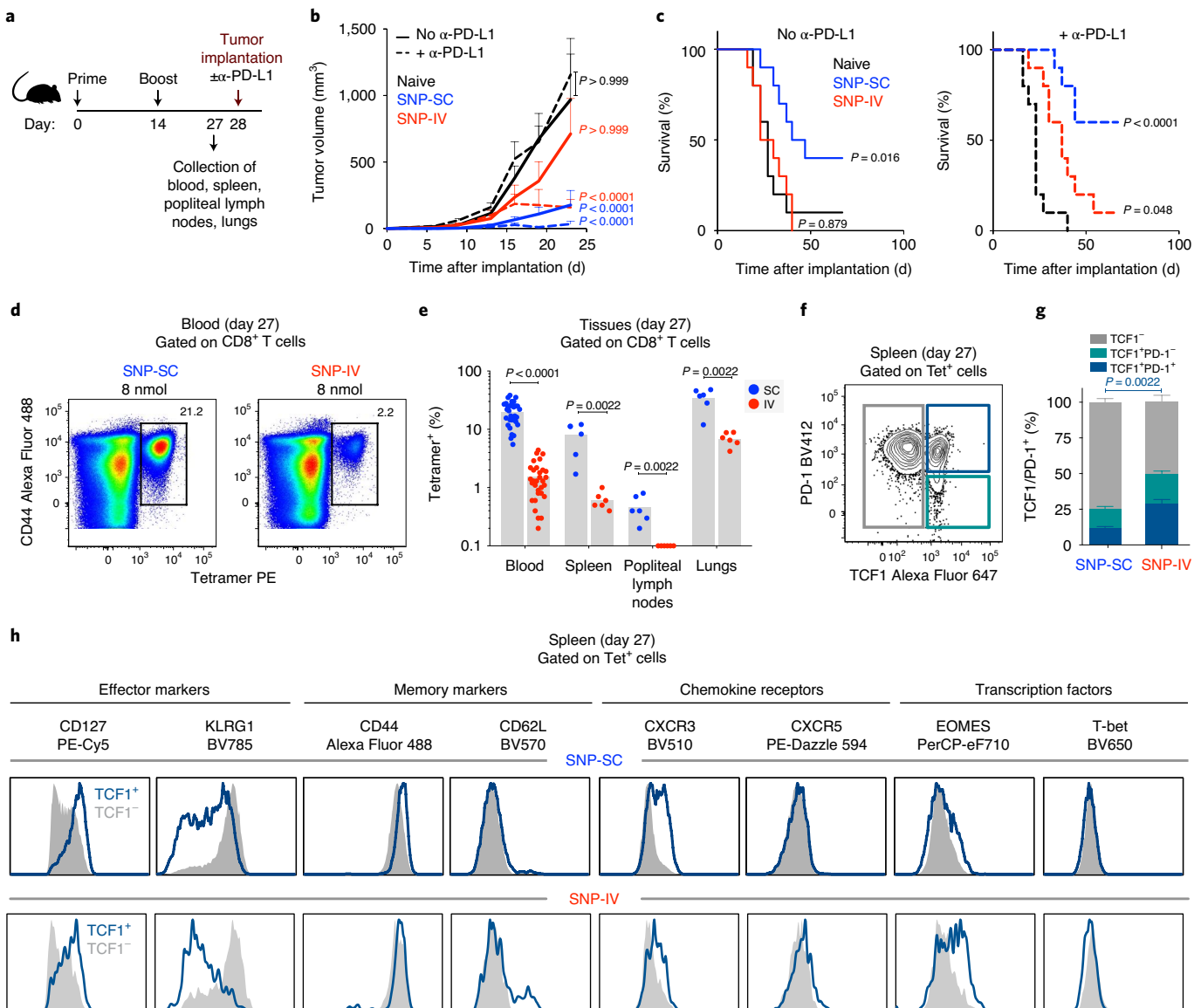


Fig. 2 | IV administration of SNP-7/8a generates TCF1 $^+$ CD8 $^+$ T cells with antitumor capacity on anti-PD-L1 treatment. **a**, Mice ($n=16$) were vaccinated subcutaneously or intravenously with SNP-7/8a (RepS1). Whole blood, spleen, popliteal lymph nodes and lungs were collected before tumor implantation on day 28. **b,c**, Tumor growth curves (**b**) and Kaplan-Meier survival curves (**c**) of unvaccinated mice (black) or vaccinated with SNP-SC (blue) or SNP-IV (red), with (dotted line) or without (solid line) $\alpha\text{-PD-L1}$ ($n=13$). **d**, Flow cytometry analysis of single cells stained with the RepS1 tetramer and CD44 antibody. The numbers indicate the percentage of the cell population within the gate. **e**, Frequency of tetramer $^+$ CD8 $^+$ T cells from blood ($n=32$), spleen, popliteal lymph nodes and lungs ($n=6$) on day 27 after vaccination. **f**, Effector CD8 $^+$ T cells in the spleen were subdivided into TCF1 $^-$ (gray), TCF1 $^+\text{PD-1}^-$ (teal) or TCF1 $^+\text{PD-1}^+$ (dark blue) populations. **g**, Bar graphs summarizing the frequencies of TCF1 subpopulations in the spleen ($n=6$) after SNP-SC or SNP-IV. **h**, Histograms showing the differential expression of phenotypic markers expressed by TCF1 $^+$ (dark blue) or TCF1 $^-$ (gray) populations after SNP-SC (top) or SNP-IV (bottom) as assessed by flow cytometry (concatenated, $n=6$). Data are representative of four independent experiments. **b,e,g**, The mean \pm s.e.m. are shown. **b**, **e,g**, Statistics were assessed by two-way ANOVA with Bonferroni correction. **c**, Statistics were assessed by log-rank test. **e,g**, Statistics were assessed by Mann-Whitney U-test.

In this study, we demonstrate how altering the route and dose of vaccination with SNP-7/8a influences the magnitude, transcriptional quality and antitumor capacity of neoantigen-specific CD8 $^+$ T cells. In addition, we identify the innate mechanisms for how the route of vaccination alters antigen duration and tropism for distinct DC subsets critical for imprinting CD8 $^+$ T cell responses.

Results

Route and dose of SNP-7/8a immunization alter the magnitude and quality of neoantigen $^+$ CD8 $^+$ T cells. SNP-7/8a is a self-assembling nanoparticle vaccine platform that standardizes the

delivery of LPs¹¹ (Fig. 1a). In this study, we determined how modifying the dose and route of SNP-7/8a immunization influenced CD8 $^+$ T cell responses. Mice were vaccinated with SNP-7/8a containing RepS1, an MC38 murine colon carcinoma neoantigen (Fig. 1b). Whole blood was collected to measure neoantigen-specific CD8 $^+$ T cells by tetramer staining (Fig. 1c and Extended Data Fig. 1a) or IFN- γ after restimulation with RepS1 peptide (Extended Data Fig. 1b). At a dose of 8 nmol, subcutaneous administration of SNP-7/8a (SNP-SC) generated 20-fold higher neoantigen-specific CD8 $^+$ T cells compared to intravenous vaccination (SNP-IV) (Fig. 1d). CD4 $^+$ T cells produced IFN- γ at low frequencies as described previously¹¹

(Extended Data Fig. 1c). Together, these data show that the route of vaccination alters the magnitude of the CD8⁺ T cell response.

Next, we characterized CD8⁺ memory precursor effector cells (MPECs) or short-lived effector cells (SLECs) based on the differential expression of CD127 (IL-7R) and KLRG1 (Fig. 1e). A high proportion of neoantigen-specific CD8⁺ T cells after SNP-SC were SLECs (approximately 60% of tetramer⁺) whereas SNP-IV cells were primarily MPECs (approximately 60% of tetramer⁺) (Fig. 1f and Extended Data Fig. 1d). The frequency of MPECs was inversely correlated to the frequency of tetramer⁺ CD8⁺ T cells (Fig. 1g and Extended Data Fig. 1e). We then assessed the expression of PD-1 and Tim-3, canonical markers of T cell activation, exhaustion or severe dysfunctionality³³ (Fig. 1h). Tetramer⁺ CD8⁺ T cells from both SNP-SC and SNP-IV mice were PD-1⁺ but only the SC-vaccinated groups expressed low levels of Tim-3 (Fig. 1i and Extended Data Fig. 1f). Peptide restimulation markedly increased the expression of PD-1 and Tim-3 after SNP-SC but not SNP-IV (Fig. 1j and Extended Data Fig. 1g). Taken together, the data suggest that the route of vaccination influences the differentiation of neoantigen-specific CD8⁺ T cells.

IV administration of SNP-7/8a generates TCF1⁺PD-1⁺CD8⁺ T cells with antitumor capacity on anti-PD-L1 treatment. To investigate the antitumor capacity of neoantigen-specific CD8⁺ T cells, mice were challenged with MC38 tumors (Fig. 2a). To evaluate the effect of a CPI, mice were also treated with or without anti-PD-L1. Anti-PD-L1 treatment alone was not sufficient to control tumor growth in unvaccinated mice (Fig. 2b and Extended Data Fig. 2a) or extend survival (Fig. 2c). SNP-SC-vaccinated mice significantly controlled tumor growth compared to naive mice (Fig. 2b) independent of CPI treatment. Despite the tenfold reduction in CD8⁺ T cell responses (Fig. 2d), SNP-IV-vaccinated mice were able to control tumor growth (Fig. 2b) and had extended survival compared to naive mice (Fig. 2c) only when combined with CPI treatment.

The distribution of tetramer⁺ CD8⁺ T cells was assessed at the time of tumor challenge in the blood, spleen, popliteal lymph nodes (SC vaccine-draining) and lungs (Fig. 2e). Neoantigen-specific CD8⁺ T cells generated by SNP-SC were significantly higher in all tissues compared to SNP-IV. We detected a population of TCF1⁺PD-1⁺ within tetramer⁺ cells in the spleen (Fig. 2f). Such cells have been described in chronic LCMV¹⁵ as a population of exhausted cells that retain proliferative capacity. SNP-IV generated a higher proportion of TCF1⁺ cells, representing approximately 50% of tetramer⁺ CD8⁺ T cells (Fig. 2g). TCF1⁺ cells in the SNP-IV group exhibited high CD127 and low KLRG1 (Fig. 2h). TCF1⁺CD8⁺ T cells generated by SNP-IV also expressed proteins upregulated by Tex progenitor cells that retained a stem-like program^{15,18,27} such as eomesodermin (EOMES) and CXCR3 (Fig. 2h). However, CXCR5 expressed by stem-like cells after chronic LCMV was not detected in TCF1⁺CD8⁺ T cells after SNP-7/8a vaccination. As a staining control, CD4⁺ follicular helper T (T_{FH}) cells expressed CXCR5 (Extended Data Fig. 2b). In contrast, TCF1⁺CD8⁺ T cells generated by SNP-SC had high expression of KLRG1 and lower EOMES levels (Fig. 2h). To assess

the generalizability of these observations, mice were immunized with SNP-7/8a containing other antigens including E7, ovalbumin and Trp1 (Extended Data Fig. 2c). Similarly, SNP-IV resulted in lower magnitude responses (Extended Data Fig. 2d) but a higher frequency of TCF1⁺PD-1⁺ cells (Extended Data Fig. 2e,f) and MPECs (Extended Data Figs. 2g,h) compared to SNP-SC, regardless of the antigen. These data indicate a phenotypic difference in the neoantigen-specific CD8⁺ T cells generated depending on the route of vaccination.

Single-cell analysis of neoantigen-specific CD8⁺ T cells identifies a stem-like gene signature after SNP-IV. To further characterize neoantigen-specific CD8⁺ T cells, we sorted tetramer⁺ cells after SNP-SC or SNP-IV vaccination (Fig. 3a and Extended Data Fig. 3a). Tetramer⁺ CD8⁺ T cells from individual mice were barcoded before single-cell RNA sequencing (scRNA-seq) using the droplet-based system of 10x Genomics (Extended Data Fig. 3b). Cells were clustered based on gene expression using an unsupervised inference analysis (Monocle 3). The 12 clusters identified were visualized by uniform manifold approximation and projection for dimension reduction (UMAP) algorithm (Fig. 3b). Clustering data showed separation of single cells by route of vaccination (Fig. 3c and Extended Data Fig. 3c). SNP-IV neoantigen⁺ cells were primarily in clusters 2 and 4, which we refer to as ‘stem-like’ cells given that *Tcf7* (encoding TCF1) was a significant differentially expressed gene (DEG) in these two clusters (Fig. 3d and Supplementary Table 1). In contrast, SNP-SC neoantigen⁺ cells mainly appeared in the ‘effector’ cluster consisting of clusters 1, 3, 5, 7 and 8 (Fig. 3d). Both stem-like and effector clusters formed stable states (high-density areas on UMAP)³⁴ (Extended Data Fig. 3d). Cluster 10 represents a small population of naive T cells (*Ccr7*, *Lef1*, *Sell*, *Dapl1*, *Igfbp4*) (Extended Data Fig. 3e) that may have been contaminated while sorting due to low frequencies with SNP-IV. Excluding naive cells, the T cell receptor (TCR) repertoire was largely diverse after both routes of immunization (Extended Data Fig. 3f). The fraction of stem-like or effector cells within each clone was driven by the route of vaccination, rather than clonotype identity (Extended Data Fig. 3g).

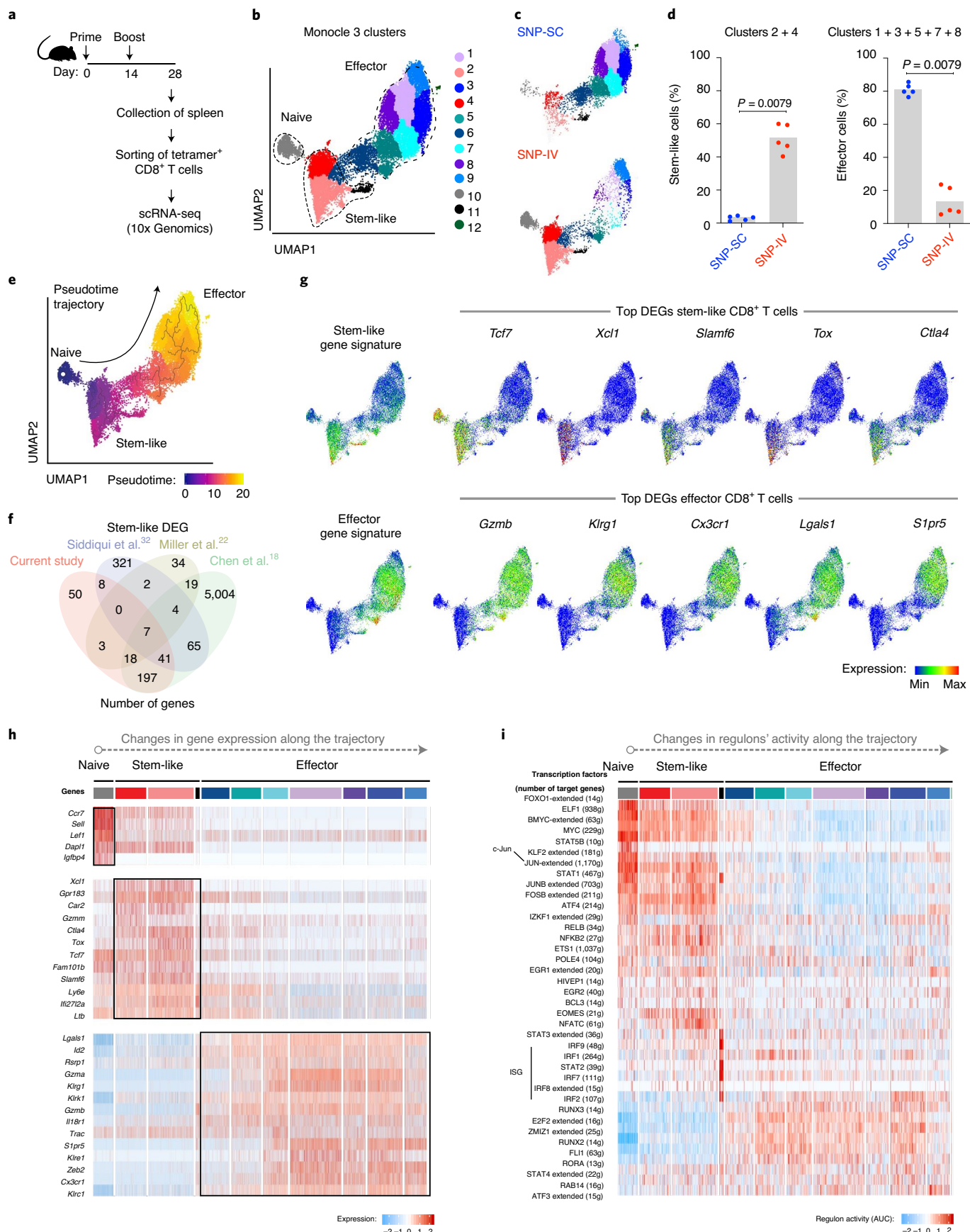
Next, we reconstructed a developmental trajectory of neoantigen-specific CD8⁺ T cells. The pseudotime analysis showed a trajectory originating from naive T cells, branching into stem-like cells and eventually effector cells (Fig. 3e). We further compared stem-like cells in this study with published datasets from chronic LCMV or tumor models^{18,22,32}, identifying 337 shared genes and 50 unique genes in our dataset (Fig. 3f and Supplementary Table 2). Applying a list of previously described stem-like genes (also referred to as ‘Tex progenitors’) and effector genes (T_{eff}) in the context of LCMV infection¹⁸, we confirmed that the stem-like gene signature was highly expressed in clusters 2 and 4, whereas the effector gene signature was more pronounced in clusters 1, 3, 5, 7 and 8 (Fig. 3g).

Consistent with flow cytometry detection of TCF1 in SNP-IV CD8⁺ T cells (Fig. 2f), the stem-like cluster expressed high levels of *Tcf7* (Fig. 3g). These cells also expressed genes associated with T cell exhaustion—*Tox*, *Lag3* and *Ctla4*—yet upregulated antiapoptotic genes such as *Bcl2* (Supplementary Table 2). As previously observed

Fig. 3 | Single-cell analysis of neoantigen⁺ CD8⁺ T cells by RNA-seq identifies stem-like gene signature in SNP-IV cells and an effector gene signature in SNP-SC cells. **a**, Mice ($n=5$) were vaccinated subcutaneously or intravenously with SNP-7/8a (Reps1). Spleens were collected on day 28 and tetramer⁺ CD8⁺ T cells were sorted by flow cytometry. scRNA-seq was performed by 10x Genomics. **b**, UMAP of sorted neoantigen⁺ CD8⁺ T cells from spleens. Twelve clusters were generated by Monocle 3 ($k=12$) analysis of gene expression. **c**, Single cells from SNP-IV (top) or SNP-SC (bottom) clusters in distinct regions of the UMAP space. **d**, Bar graphs summarizing the frequencies of stem-like cells (clusters 2 and 4, left) or effector cells (clusters 1, 3, 5, 7 and 8, right) of total tetramer⁺ CD8⁺ T cells in the spleen ($n=5$). **e**, Reconstruction of pseudotime trajectory using the Monocle 3 algorithm. **f**, Venn diagram comparing the identified DEGs of stem-like cells in this study and three published datasets. **g**, The lists of stem-like or effector gene signatures were overlaid on the UMAP of single-cell data. The expression of the top DEGs of stem-like (top) or effector (bottom) cells is presented as UMAP plots. **h**, Heatmap of selected DEGs expressed in each cluster organized along the pseudotime trajectory. **i**, Heatmap of significant changes in regulons' activity as inferred by SCENIC analysis. AUC, area under the curve. **j**, Statistics were assessed by Mann-Whitney U-test.

in stem-like CD8⁺ T cells from chronic LCMV^{18,19,35}, *Slamf6* (encoding Ly108) was highly expressed in the stem-like CD8⁺ T cells after IV vaccination. Unlike data from LCMV studies, the stem-like

CD8⁺ T cells reported in this study did not show increased *Cxcr5*, which is consistent with the flow cytometry data (Supplementary Table 2 and Extended Data Fig. 3h). The stem-like cluster expressed



high levels of *Xcl1*, which encodes for XCL1, the ligand for XCR1⁺ conventional type 1 DCs (cDC1s). The effector cluster expressed genes encoding cytotoxic granules, such as *Gzma* and *Gzmb*, as well as inhibitory receptors such as *Klrg1* (Fig. 3h and Supplementary Table 1). The chemokine receptor *Cx3cr1* expressed by transitory, effector-like cells in chronic LCMV^{19,35}, was also highly expressed in our effector cluster. Other notable genes that were highly expressed in the effector cluster include *Zeb2* (triggers cytotoxic T lymphocytes to adopt a terminally differentiated state³⁶), *Lgals1* (galectin-1, a proapoptotic molecule³⁷) and *S1pr5* (*S1PR5*, cues the exit from lymphoid tissue³⁸) (Fig. 3g,h).

To further evaluate cellular states based on the expression of transcription factors and target genes, we measured the activity of regulons by performing SCENIC (single-cell regulatory network inference and clustering) analysis³⁴ (Fig. 3i). Changes in the transcriptional network were detected along the Monocle 3 pseudo-time trajectory. Upregulation of the EOMES regulon (*Eomes* and 21 related genes) was measured in the stem-like cluster, in line with EOMES detected by flow cytometry (Fig. 2h). In contrast, the effector cluster was marked by upregulation of several regulons including Runx3, Runx2, Rora and Fli1 (Fig. 3i). Taken together, at the transcriptional level, the neoantigen-specific CD8⁺ T cells generated by SNP-IV expressed a stem-like gene signature, whereas SNP-SC cells expressed an effector gene signature. Further, trajectory inference analysis of scRNA-seq data highlighted differences in the developmental states of stem-like and effector CD8⁺ T cells.

Therapeutic vaccination by SNP-IV, but not SNP-SC, controls tumor growth. To assess the antitumor capacity of SNP-7/8a in mice with established tumors, MC38 was implanted and vaccination was administered on days 7 (prime) and 14 (boost) (Fig. 4a). Anti-PD-L1 was given at the time of boost. In this study, the dose of SNP-IV was increased to 32 nmol to generate CD8⁺ T cells of comparable magnitude to the SNP-SC mice (Fig. 4b). Both vaccination routes resulted in approximately 10% Reps1⁺CD8⁺ T cells (Fig. 4c). Despite similar numbers of neoantigen-specific CD8⁺ T cells, SNP-SC mice could not control tumor growth whereas SNP-IV mice significantly controlled tumor growth compared to naive mice (Fig. 4d). The antitumor efficacy of SNP-IV was antigen-specific and adjuvant-dependent since vaccinating with an irrelevant antigen intravenously (Fig. 4e) or no adjuvant (SNP with no TLR7/8a) (Extended Data Fig. 4a) was ineffective. The differences in tumor growth was further confirmed by the prolonged survival of mice vaccinated with SNP-IV but not SNP-SC (Fig. 4f). Decreasing the SNP-SC dose or reducing to a single vaccination was not effective (Extended Data Fig. 4b). Tumor control (Fig. 4g) and increased survival (Fig. 4h) by SNP-IV were abrogated by depleting CD8⁺ T cells but not CD4⁺ T cells or natural killer cells (Extended Data Fig. 4c,d).

To delineate each variable of the SNP-IV treatment regimen, MC38 tumor-bearing mice were vaccinated on day 7 with 32 nmol of SNP containing Reps1 (Fig. 4i). On day 14, groups of mice were either left untreated ('prime'), given CPI ('prime and CPI'), vaccinated again ('prime and boost') or vaccinated again together with

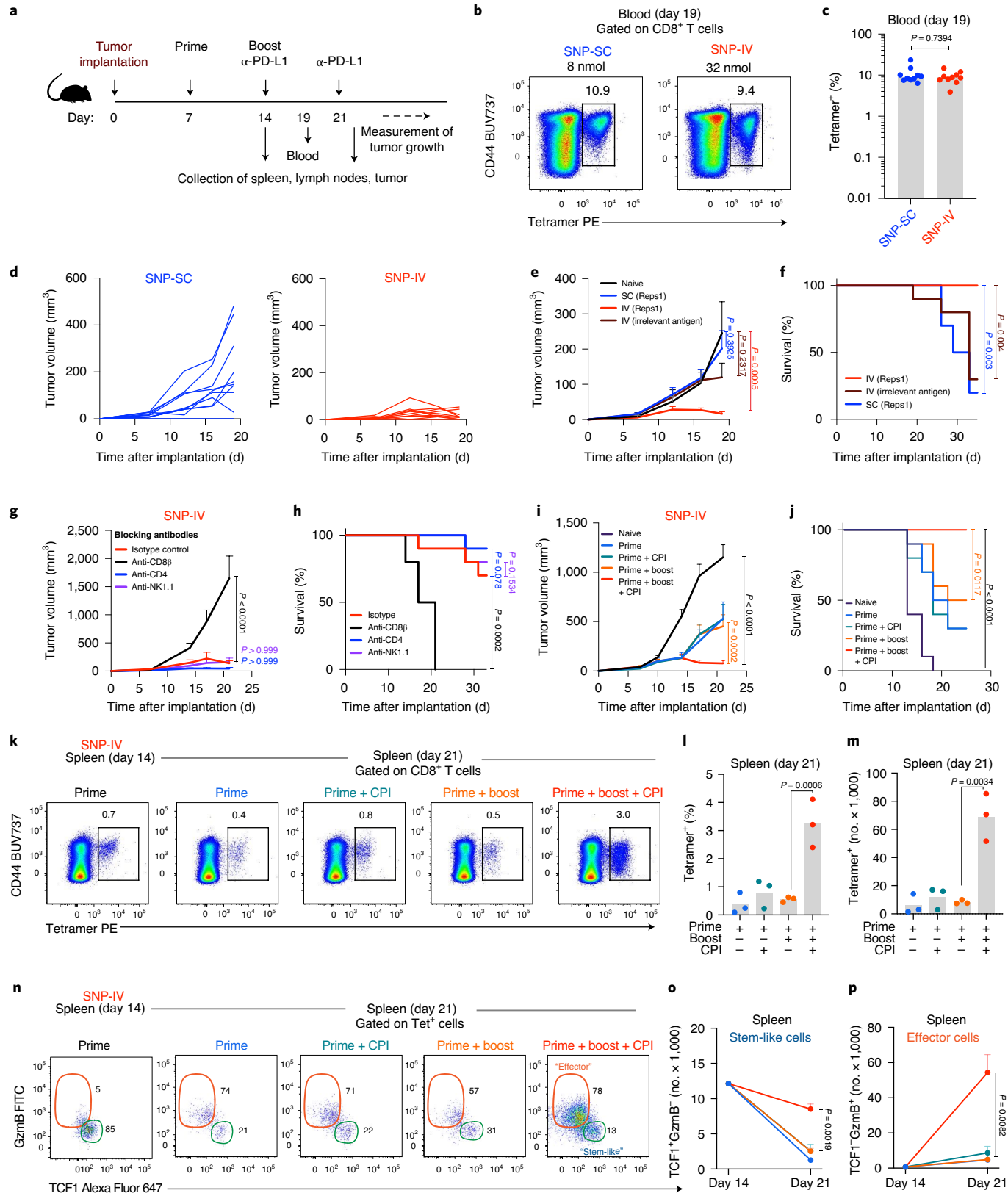
CPI ('prime, boost and CPI'). Indeed, the combination of both vaccinations and CPI was most effective at controlling tumor growth (Fig. 4i) and extending survival (Fig. 4j). Spleens were collected from mice on day 14 (post-prime) and day 21 after tumor implantation (Fig. 4k). Without the boost or CPI treatment, the frequency of neoantigen-specific CD8⁺ T cells in the spleen was significantly lower (sixfold) than mice that received a boost and CPI (Fig. 4l). A clear expansion of neoantigen-specific CD8⁺ T cells was observed when enumerating tetramer⁺ CD8⁺ T cells in the spleen on day 21 (Fig. 4m). On day 14, approximately 80% of CD8⁺ T cells were stem-like (TCF1⁺GzmB⁻) after SNP-IV, compared to 35% after SNP-SC (Fig. 4n). Co-staining with PD-1 confirmed that these cells were high in PD-1 (Extended Data Fig. 4e). By day 21 post-SNP-IV, neoantigen⁺ CD8⁺ T cells from the spleens of tumor-bearing mice had mostly differentiated to effector cells (TCF1⁺GzmB⁺) (Fig. 4n). Mice receiving both immunizations and CPI maintained high numbers of stem-like cells in the spleen (Fig. 4o) unlike the other groups that did not receive a boost or CPI. This coincided with a significant tenfold increase in neoantigen⁺ effector cells expressing granzyme B (GzmB) in mice that received boost and CPI, compared to mice that received boost with no CPI (Fig. 4p). In contrast, a modest 1.5-fold expansion of effector cells in the spleen was observed after SNP-SC (Extended Data Fig. 4f). Importantly, neoantigen-specific CD8⁺ T cells generated by SNP-SC coexpressed PD-1 and Tim-3 by day 21 (approximately 35%) while SNP-IV cells did not express Tim-3 in the spleen (Extended Data Fig. 4g). On day 21, SNP-IV cells had increased Ki-67 expression in blood and spleen (Extended Data Fig. 4h), indicating an expansion of circulating effector cells. Taken together, these results highlight the capacity of stem-like neoantigen⁺ CD8⁺ T cells generated by SNP-IV to proliferate and replenish effector cells for antitumor responses upon CPI treatment.

Prolonged antigen persistence, DC uptake and activation after SNP-SC but not SNP-IV. To investigate differences in the mechanism of CD8⁺ T cell priming, fluorescently labeled SNP-7/8a was used to visualize the distribution and uptake by DCs. In vivo imaging of mice revealed that SNP-SC was localized to the site of vaccination two weeks after vaccination, highlighting a depot effect (Extended Data Fig. 5a). In contrast, SNP-IV resulted in systemic distribution of the vaccine detectable up to 24 h by in vivo imaging (Extended Data Fig. 5a). Lymph node sections analyzed by confocal microscopy confirmed that vaccine could be detected up to two weeks after SNP-SC, primarily in the T cell zones (Fig. 5a and Extended Data Fig. 5b). Co-staining with monocyte, macrophage and DC markers revealed colocalization of vaccine with cells expressing CD11b and CD11c (Extended Data Fig. 5c). After SNP-IV, confocal images of spleen sections showed vaccine uptake by CD11b⁺CD11c⁺ cells situated in the marginal zones primarily after 6 and 24 h with minimal vaccine detection after 3 and 7 d (Fig. 5b). Popliteal lymph nodes and spleens were collected for flow cytometry analysis (Extended Data Fig. 5d). Labeled vaccine could be detected in both cDC1s (Lin⁻MHC-II⁺CD11c⁺XCR1⁺) and monocyte-derived DCs (Lin⁻CD64⁺F4/80⁺MHC-II⁺CD11c⁺)

Fig. 4 | Therapeutic vaccination with SNP-IV generates neoantigen-specific CD8⁺ T cells with superior antitumor capacity. **a**, Mice ($n=10$) were implanted with MC38, vaccinated with SNP-7/8a (Reps1) and treated with CPI. **b,c**, Flow analysis of blood stained with tetramer and CD44 antibody ($n=10$). **d**, Tumor growth in SNP-SC or SNP-IV mice ($n=10$). **e,f**, Average tumor growth (**e**) and survival (**f**) of Reps1 IV (red), irrelevant IV (maroon), Reps1 SC (blue) and unvaccinated (black) mice. **g,h**, Average tumor growth (**g**) and survival (**h**) of SNP-IV mice treated with isotype (red) or blocking antibodies against CD8⁺ (black), CD4⁺ (blue) and natural killer cells (purple) ($n=10$). **i,j**, Average tumor growth (**i**) and survival (**j**) of mice vaccinated with SNP-IV once (blue), vaccinated once and given CPI (green), vaccinated twice (orange), vaccinated twice and given CPI (red) or untreated (black) ($n=10$). **k**, Flow cytometry analysis of spleens stained with tetramer and CD44 antibody. **l,m**, Frequency (**l**) and total number (**m**) of tetramer⁺ CD8⁺ T cells on day 21 ($n=3$). **n**, Flow cytometry analysis of spleens stained with TCF1 and GzmB. FITC, fluorescein isothiocyanate. **o,p**, Total number of stem-like cells (TCF1⁺GzmB⁻) (**o**) and effector cells (TCF1⁺GzmB⁺) (**p**) on day 21 ($n=3$) (unpaired t-test). Data are representative of four independent experiments. **c**, The bars represent the median. **l,m**, The bars represent the mean \pm s.e.m. **e,g,i**, Statistics were assessed by Mann-Whitney U-test. **e,g,i**, Statistics were assessed by two-way ANOVA. **f,h,j**, Statistics were assessed by log-rank test. **l,m,o,p**, Statistics were assessed by two-tailed unpaired t-test.

in the popliteal lymph nodes after SNP-SC as late as 3 weeks after vaccination (Fig. 5c and Extended Data Fig. 5e). Similarly, SNP-IV resulted in uptake by cDC1s and monocyte-derived DCs in the spleen. However, this peaked at 6 h after vaccination (Fig. 5c and

Extended Data Fig. 5f). The costimulatory molecules CD80 and CD86 as well as the regulatory marker PD-L1 were upregulated in cDC1s and monocyte-derived DCs after vaccination by both routes (Fig. 5d). SNP-IV resulted in transient DC activation that peaked



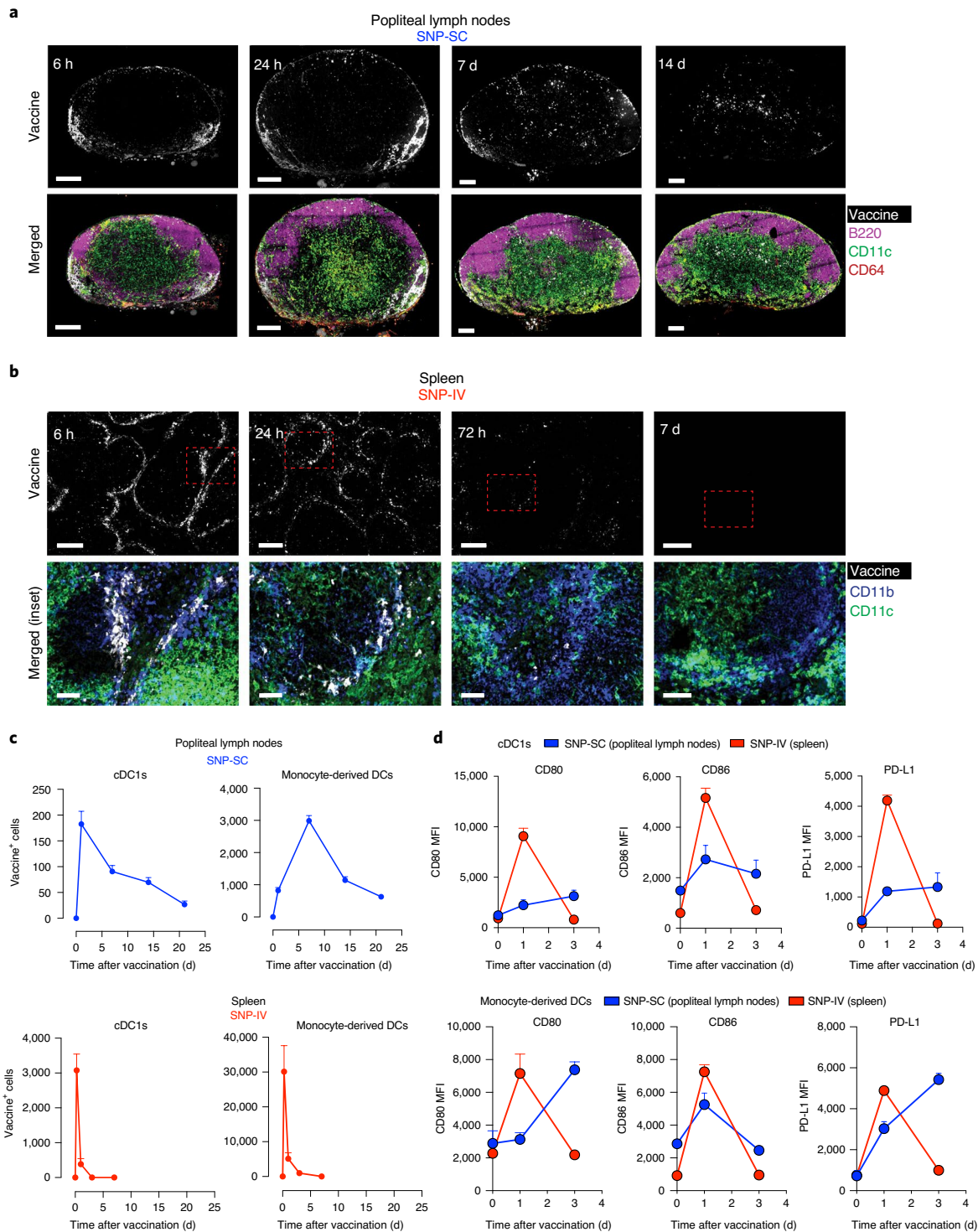


Fig. 5 | Transient vaccine distribution to the spleen and activation of migratory cDC1s and monocyte-derived DCs after SNP-IV. **a**, Mice ($n=3$) were vaccinated with SNP-7/8a labeled with Alexa Fluor 647. Popliteal lymph nodes and spleens were collected from mice at specified time points. Confocal images of sections from popliteal lymph nodes collected at 6 and 24 h and at 7 and 14 d after SC injection with labeled SNP-7/8a are shown. Top, vaccine. Bottom, merged. White, vaccine; magenta, B220 (B cells); green, CD11c (monocyte-derived DCs or cDCs); red, CD64 (monocytes or macrophages). Scale bars, 200 μ m. **b**, Confocal images of sections from spleens collected at 6 and 24 h and at 3 and 7 d after IV injection with labeled SNP-7/8a are shown. Top, vaccine. Bottom, merged of inset. White, vaccine; blue, CD11b (monocytes, macrophages or cDC2s); CD11c (monocyte-derived DCs or cDCs). Scale bars, 200 μ m or 50 μ m (inset). **c**, Popliteal lymph nodes and spleens were collected and single-cell suspensions were assessed by flow cytometry for detailed identification of DC subsets. Kinetics of vaccine⁺ cDC1s (XCR1⁺MHC-II⁺CD11c⁺, left) and monocyte-derived DCs (F4/80⁺CD64⁺MHC-II⁺CD11c⁺, right) in popliteal lymph nodes (top) or spleen (bottom) after injection with labeled vaccines via SC or IV, respectively ($n=3$). **d**, Graphs summarizing the mean fluorescence intensity (MFI) of CD80 (left), CD86 (middle) and PD-L1 (right) expressed on cDC1s and monocyte-derived DCs in popliteal lymph nodes after SNP-SC (blue lines) or in the spleen after SNP-IV (red lines) ($n=3$). Mean \pm s.e.m. **c,d**, Data are representative of two independent experiments.

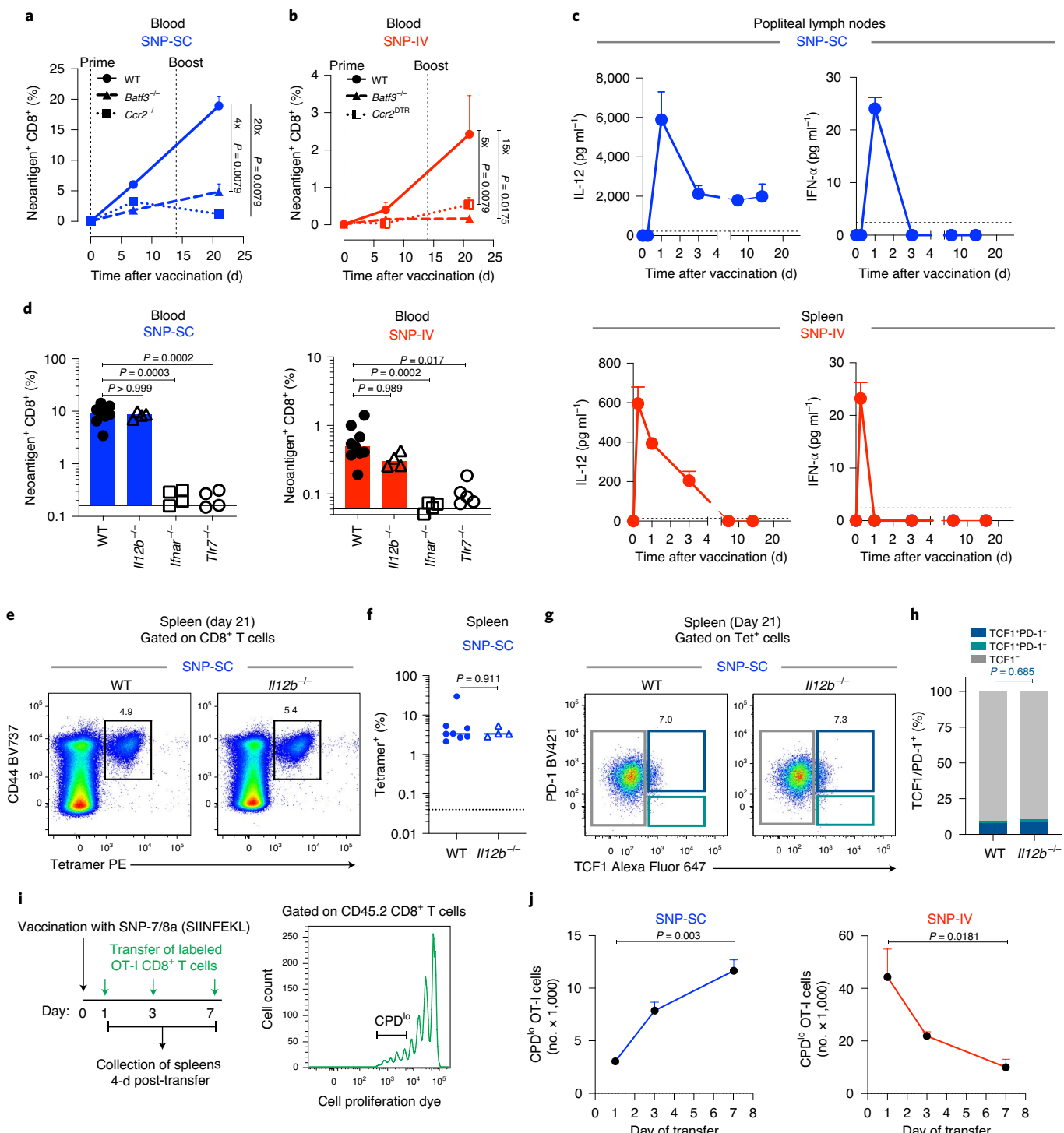


Fig. 6 | Prolonged antigen presentation by DCs drives CD8⁺ T cell responses after SNP-SC. **a,b**, Kinetics of neoantigen-specific CD8⁺ T cells after SNP-SC (**a**) or SNP-IV (**b**) in $\text{Batf3}^{-/-}$ (triangle), $\text{Ccr2}^{-/-}$ (square) and Ccr2^{DTR} treated with diphtheria toxin (half square) as compared to WT mice (circle) ($n=10$). **c**, IL-12 (left) and IFN- α (right) were measured by ELISA in the supernatants of cultured spleens or popliteal lymph nodes after SNP-IV or SNP-SC, respectively ($n=3$). **d**, Bar graphs summarizing neoantigen-specific CD8⁺ T cells after SNP-SC in WT mice (circle) ($n=8$), $\text{II}12b^{-/-}$ (open triangle), $\text{Ifnar}^{-/-}$ (open square) ($n=5$), $\text{Tlr7}^{-/-}$ (open circle) ($n=5$). **e,f**, Flow analysis of splenocytes stained with CD44 antibody (**e**) and tetramer (**f**) after SNP-SC in WT ($n=8$) or $\text{II}12b^{-/-}$ ($n=4$) mice. **g,h**, CD8⁺ T cells in the spleen after SNP-SC were subdivided into TCF1⁺ (gray), TCF1⁺PD-1⁻ (teal) or TCF1⁺PD-1⁺ (dark blue) (**g**). The bar graphs summarize the frequencies of TCF1 subpopulations ($n=4$) (**h**). **i**, CD45.1 mice ($n=3$) were vaccinated with SNP-7/8a (SIINFEKL). 1, 3 or 7 d after vaccination, naive CD8⁺ T cells from CD45.2 OT-I mice were labeled and transferred into CD45.1 mice. Four days after transfer, spleens were assessed for cell proliferation. **j**, Graphs summarizing the number of CPD¹⁰ cells after SNP-SC (left) or SNP-IV (right) ($n=3$). Data are representative of two independent experiments. **a–c,j**, The bars represent the mean \pm s.e.m. **a,b,j**, Statistics were assessed by Mann-Whitney U-test. **d**, Statistics were assessed by Kruskal-Wallis test with Dunn's correction for multiple comparisons.

at day 1, whereas SNP-SC resulted in prolonged activation of DCs over 3 d (Fig. 5d). Expression of CD80, CD86 and the migratory marker CCR7 on monocyte-derived DCs were detectable 3 weeks later suggesting continued infiltration of antigen-presenting cells (APCs) into the draining lymph nodes (Extended Data Fig. 5g). The frequency of cDC1s in the spleen after SNP-IV peaked at 6 h and diminished to below baseline levels at 24 h as assessed by flow cytometry (Extended Data Fig. 5h,i). In contrast, the numbers of cDC1s remained high three weeks after SNP-SC in the popliteal lymph nodes (Extended Data Fig. 5h,i). The differences in the presence and activation of cDC1s at the site of priming highlight the potential importance of DCs in modulating CD8⁺ T cell quality after SNP vaccination.

cDC1s and monocyte-derived DCs are required for CD8⁺ T cell priming. To directly address the role of specific APCs in priming CD8⁺ T cells, wild-type (WT), *Batf3*^{-/-} and *Ccr2*^{-/-} mice lacking cross-presenting cDC1s and circulating monocytes, respectively were immunized with SNP-7/8a (Extended Data Fig. 6a,b). The frequency of neoantigen-specific CD8⁺ T cells was significantly decreased after SNP-SC in *Batf3*^{-/-} (fourfold lower) and *Ccr2*^{-/-} (20-fold lower) mice (Fig. 6a). Since monocytes remain in the spleens of *Ccr2*^{-/-} mice, we generated bone marrow chimeras of *Ccr2*^{DTR} mice to conditionally deplete monocytes in peripheral tissues and lymphoid organs (Extended Data Fig. 6c,d). After SNP-IV, the frequency of neoantigen-specific CD8⁺ T cells significantly decreased by diphtheria toxin treatment of *CCR2*^{DTR} bone marrow chimera mice (fivefold lower) and *Batf3*^{-/-} mice (15-fold lower) suggesting dependency on monocytes and cDC1s (Fig. 6b). Mice receiving WT bone marrow with or without diphtheria toxin treatment and mice receiving *Ccr2*^{DTR} bone marrow without diphtheria toxin treatment generated similar frequencies of neoantigen-specific CD8⁺ T cells after SNP-IV (Extended Data Fig. 6e). Collectively, these data highlight a critical role for not only BATF3-dependent cDC1s but also monocyte-derived DCs in priming CD8⁺ T cells with the SNP-7/8a vaccine.

Since type I IFN (promoting cross-presentation³⁹) and IL-12 (promoting T_H1 skewing⁴⁰) can have critical roles in controlling CD8⁺ T cell priming, these cytokines were measured. SNP-IV induced transient production of IL-12 and IFN- α , which peaked at 6 h after vaccination in blood and spleen (Fig. 6c and Extended Data Fig. 6f). In contrast, IL-12 was detected up to 2 weeks after SNP-SC in the popliteal lymph nodes (Fig. 6c), which is consistent with the duration of vaccine detection (Fig. 5a).

To investigate the importance of IL-12 and IFN- α , *Il12b*^{-/-} and *Ifnar*^{-/-} mice were vaccinated (Fig. 6d), with *Tlr7*^{-/-} mice used as a negative control. Both priming and boosting of neoantigen-specific CD8⁺ T cells with SNP-SC or SNP-IV were IFN- α - and TLR7-dependent but IL-12-independent (Fig. 6d). In mice deficient for IFN- α receptor and TLR7, fewer monocytes and cDC1s were in the popliteal lymph nodes after SNP-SC than in WT mice (Extended Data Fig. 6g). To assess whether IL-12 affected the quality of neoantigen⁺ CD8⁺ T cells²¹, we collected spleens after SNP-SC boost. Similar to blood responses, *Il12b*^{-/-} mice had comparable tetramer⁺ CD8⁺ T cell responses in the spleen as WT mice after SNP-SC (Fig. 6e,f). Further, similar frequencies of TCF1 in both *Il12b*^{-/-} and WT neoantigen⁺ CD8⁺ T cells suggest that IL-12 signaling was not mediating TCF1 downregulation (Fig. 6g,h). EOMES expression was higher in *Il12b*^{-/-} compared to WT mice after SNP-SC (Extended Data Fig. 6h).

SNP-SC leads to prolonged antigen retention and presentation in vivo. Based on the data showing prolonged retention of vaccine and innate activation after SC immunization (Fig. 5c,d), we hypothesized that antigen persistence mediated the differences in CD8⁺ cell quality between SC and IV vaccination. Naive CD45.2 OT-I

CD8⁺ T cells were labeled with a fluorescent dye and transferred to CD45.1 congenic mice 1, 3 or 7 d after vaccination with SNP-7/8a delivering the OT-I peptide (SIINFEKL) (Fig. 6i). Spleens were collected 4 d after cell transfer to assess the extent of CD8⁺ T cell proliferation as an indicator of antigen presence. At all three time points, cell proliferation could be detected, with the largest numbers of OT-I measured being 7 d after SNP-SC vaccination (Fig. 6j). In contrast, SNP-IV resulted in a burst of OT-I expansion when transferred 1 d after vaccination followed by significantly lower cell numbers 3 and 7 d after vaccination (Fig. 6j). Overall, the prolonged persistence of antigen in the popliteal lymph nodes drove T cell differentiation, thus explaining the high magnitude but lower proliferative potential of neoantigen-specific CD8⁺ T cells generated by SNP-SC.

Discussion

In this study, we report how SNP-7/8a dose and route control the magnitude and transcriptional quality of neoantigen-specific CD8⁺ T cells. In the context of cancer immunotherapy, persistence and functional capability are important factors given the chronic nature of cancer. The most striking finding was the demonstration that IV vaccination led to a major difference in the phenotypic and transcriptional quality of the CD8⁺ T cell response compared to SC vaccination. SNP-7/8a vaccination enables specific generation of stem-like or effector cells by modifying the route of vaccination. We demonstrate how this can be achieved *in vivo* using CD8⁺ T cells primed from a polyclonal naive repertoire, without the caveats of TCR transgenic systems using model antigens. We note that IV administration of RNA-based PCV has been shown to be more immunogenic than direct lymph node injection; however, the transcriptional quality of CD8⁺ T cells by this route has not been assessed^{41,42}. In this study, we clearly demonstrate that neoantigen-specific CD8⁺ T cells generated by SNP-IV have a high proportion of TCF1⁺PD-1⁻ stem-like cells and mediate antitumor effects dependent on CPI.

The scRNA-seq data of neoantigen⁺ CD8⁺ T cells revealed distinct transcriptional landscapes after SNP-SC or SNP-IV, providing insight into the dynamics of CD8⁺ T cell activation and differentiation after vaccination: naive cells give rise to stem-like cells that can be further differentiated into effector cells. Comparison of clusters revealed several new genes highly expressed by stem-like CD8⁺ T cells. *Xcl1* expression by stem-like CD8⁺ T cells suggests a role for XCR1⁺ cDC1s⁴³ in licensing their activity in the spleen. In stem-like cells, the expression of *Tox*, recently described as a crucial regulator of T cell exhaustion^{44,45}, may be beneficial in preventing overstimulation of CD8⁺ T cells leading to cell death, especially in the context of cancer where there is antigen persistence. Interestingly, neoantigen-specific CD8⁺ T cells generated by SNP-IV resemble the stem-like or progenitor exhausted cells described in chronic LCMV infection, whereas cells generated by SNP-SC share genes upregulated in acute LCMV infection^{15,18,19}. Epigenetic analysis, specifically around the *Tox* locus, may reveal whether vaccine-induced CD8⁺ T cells resemble a distinct developmental program or share specific features of exhausted cells identified in LCMV^{46,47}. Unlike chronic LCMV where there is persistent antigenic stimulation, we observed stem-like CD8⁺ T cells after IV vaccination of a peptide-based vaccine where the duration of antigenic delivery peaked at 6 h. These data suggest distinct mechanisms of CD8⁺ T cell priming in vaccination versus natural infection and demonstrate the rapidity by which such cells can be induced by the SNP-7/8a vaccine, which will be critical for therapeutic tumor vaccination.

The covalent linking of antigen and adjuvant into a nanoparticle was designed to synchronously deliver the innate stimulation with the antigen for efficient cross-presentation. Several important factors may contribute to the modulation of CD8⁺ T cell quality on IV vaccination: location of CD8⁺ T cell priming; actual dose of vaccine delivered to splenic DCs; and degree of inflammation. The

duration of antigen persistence of up to three weeks in the draining lymph nodes by SNP-SC contrasted with a short burst of antigen in the spleen by SNP-IV. Despite the brief duration, the spleen is a large reservoir for DCs as noted by the tenfold increase in absolute numbers of cDC1s or monocyte-derived DCs acquiring vaccine at the peak of SNP-IV delivery, compared to the numbers of vaccine⁺ DCs in the popliteal lymph nodes at the peak of SNP-SC delivery. This is probably the key factor in regulating the magnitude and quality of responses, respectively. In a different cancer vaccine model using peptide and incomplete Freund's adjuvant, antigen persistence also led to dysfunctional CD8⁺ T cells⁴⁸. However, it is notable in the prophylactic tumor model presented in this study, that the CD8⁺ T cells generated by SC vaccination were still highly functional. Confocal images of lymph node sections showed that, while antigen was retained for 3 weeks in the lymph nodes after SC vaccination, the localization of antigen changed: in the first 24 h, antigen was mostly in the subcapsular sinus, but over the next 2 weeks, antigen concentrated into the T cell zones. This slow-release effect has been the basis of other rational vaccine designs, regulating the kinetics of antigen exposure⁴⁹. Thus, SNP-SC was efficient at generating effector CD8⁺ T cells in high numbers. This approach may be valuable for prophylactic cancer vaccines targeting known shared tumor antigens.

Importantly, co-delivery of antigen and adjuvant permits systemic IV administration by limiting the tolerogenic effects of having free peptide taken up by APCs in the absence of a danger signal. The short-lived pharmacokinetics of SNP-IV in the spleen probably accounts for the lower magnitude when given at the same dose as SNP-SC. The reduction in numbers of splenic cDC1s between 24 h and 3 d after IV vaccination may serve as a negative immunoregulatory mechanism. Further, the dependency on monocyte-derived DCs for CD8⁺ T cell responses suggests that these cells either contribute indirectly by providing the required cytokines for T cell activation, by transferring antigen to other DCs, or directly by presenting antigens to CD8⁺ T cells. After SNP-IV, the frequency of cDC1s, the canonical subset for efficient cross-priming, were dramatically reduced. We hypothesize that monocyte-derived DCs, generally considered less efficient APCs compared to cDC1s⁵⁰, may be responsible for providing less-differentiated, more stem-like CD8⁺ T cells. Future studies should focus on how these distinct DC subsets can modify both the magnitude and quality of CD8⁺ T cells in the context of vaccination.

In conclusion, this study shows that the route of administration of the SNP-7/8a vaccine substantially affected the magnitude and transcriptional quality of neoantigen-specific CD8⁺ T cell responses, which had a corresponding impact on functionality and therapeutic outcomes. These findings have implications in the clinical development of therapeutic vaccines for cancer patients.

Online content

Any methods, additional references, Nature Research reporting summaries, source data, extended data, supplementary information, acknowledgements, peer review information; details of author contributions and competing interests; and statements of data and code availability are available at <https://doi.org/10.1038/s41590-020-00810-3>.

Received: 13 May 2020; Accepted: 16 September 2020;

Published online: 2 November 2020

References

- Rosenberg, S. A. & Restifo, N. P. Adoptive cell transfer as personalized immunotherapy for human cancer. *Science* **348**, 62–68 (2015).
- Schumacher, T. N. & Schreiber, R. D. Neoantigens in cancer immunotherapy. *Science* **348**, 69–74 (2015).
- Tumeh, P. C. et al. PD-1 blockade induces responses by inhibiting adaptive immune resistance. *Nature* **515**, 568–571 (2014).
- Versluis, J. M., Long, G. V. & Blank, C. U. Learning from clinical trials of neoadjuvant checkpoint blockade. *Nat. Med.* **26**, 475–484 (2020).
- Kreiter, S. et al. Mutant MHC class II epitopes drive therapeutic immune responses to cancer. *Nature* **520**, 692–696 (2015).
- Yadav, M. et al. Predicting immunogenic tumour mutations by combining mass spectrometry and exome sequencing. *Nature* **515**, 572–576 (2014).
- Hilf, N. et al. Actively personalized vaccination trial for newly diagnosed glioblastoma. *Nature* **565**, 240–245 (2019).
- Melief, C. J. M. Cancer: precision T-cell therapy targets tumours. *Nature* **547**, 165–167 (2017).
- Ott, P. A. et al. An immunogenic personal neoantigen vaccine for patients with melanoma. *Nature* **547**, 217–221 (2017).
- Sahin, U. et al. Personalized RNA mutanome vaccines mobilize poly-specific therapeutic immunity against cancer. *Nature* **547**, 222–226 (2017).
- Lynn, G. M. et al. Peptide-TLR-7/8a conjugate vaccines chemically programmed for nanoparticle self-assembly enhance CD8 T-cell immunity to tumor antigens. *Nat. Biotechnol.* **38**, 320–332 (2020).
- Eisenbarth, S. C. Dendritic cell subsets in T cell programming: location dictates function. *Nat. Rev. Immunol.* **19**, 89–103 (2019).
- Kaech, S. M. & Cui, W. Transcriptional control of effector and memory CD8⁺ T cell differentiation. *Nat. Rev. Immunol.* **12**, 749–761 (2012).
- McLane, L. M., Abdel-Hakeem, M. S. & Wherry, E. J. CD8 T cell exhaustion during chronic viral infection and cancer. *Annu. Rev. Immunol.* **37**, 457–495 (2019).
- Im, S. J. et al. Defining CD8⁺ T cells that provide the proliferative burst after PD-1 therapy. *Nature* **537**, 417–421 (2016).
- He, R. et al. Follicular CXCR5⁺ expressing CD8⁺ T cells curtail chronic viral infection. *Nature* **537**, 412–428 (2016).
- Snell, L. M. et al. CD8⁺ T cell priming in established chronic viral infection preferentially directs differentiation of memory-like cells for sustained immunity. *Immunity* **49**, 678–694.e5 (2018).
- Chen, Z. et al. TCF1-centered transcriptional network drives an effector versus exhausted CD8 T cell-fate decision. *Immunity* **51**, 840–855.e5 (2019).
- Hudson, W. H. et al. Proliferating transitory T cells with an effector-like transcriptional signature emerge from PD-1⁺ stem-like CD8⁺ T cells during chronic infection. *Immunity* **51**, 1043–1058.e4 (2019).
- Wu, T. et al. The TCF1-Bcl6 axis counteracts type I interferon to repress exhaustion and maintain T cell stemness. *Sci. Immunol.* **1**, eaai8593 (2016).
- Danilo, M., Chennupati, V., Silva, J. G., Siegert, S. & Held, W. Suppression of Tcf1 by inflammatory cytokines facilitates effector CD8 T cell differentiation. *Cell Rep.* **22**, 2107–2117 (2018).
- Miller, B. C. et al. Subsets of exhausted CD8⁺ T cells differentially mediate tumor control and respond to checkpoint blockade. *Nat. Immunol.* **20**, 326–336 (2019).
- Kamphorst, A. O. et al. Rescue of exhausted CD8 T cells by PD-1-targeted therapies is CD28-dependent. *Science* **355**, 1423–1427 (2017).
- Vodnala, S. K. et al. T cell stemness and dysfunction in tumors are triggered by a common mechanism. *Science* **363**, eaau0135 (2019).
- Li, H. et al. Dysfunctional CD8 T cells form a proliferative, dynamically regulated compartment within human melanoma. *Cell* **176**, 775–789.e18 (2019).
- Philip, M. et al. Chromatin states define tumour-specific T cell dysfunction and reprogramming. *Nature* **545**, 452–456 (2017).
- Brummelman, J. et al. High-dimensional single cell analysis identifies stem-like cytotoxic CD8⁺ T cells infiltrating human tumors. *J. Exp. Med.* **215**, 2520–2535 (2018).
- Sade-Feldman, M. et al. Defining T cell states associated with response to checkpoint immunotherapy in melanoma. *Cell* **175**, 998–1013.e20 (2018).
- Thommen, D. S. et al. A transcriptionally and functionally distinct PD-1⁺ CD8⁺ T cell pool with predictive potential in non-small-cell lung cancer treated with PD-1 blockade. *Nat. Med.* **24**, 994–1004 (2018).
- Jansen, C. S. et al. An intra-tumoral niche maintains and differentiates stem-like CD8 T cells. *Nature* **576**, 465–470 (2019).
- Kurtulus, S. et al. Checkpoint blockade immunotherapy induces dynamic changes in PD-1[−] CD8⁺ tumor-infiltrating T cells. *Immunity* **50**, 181–194.e6 (2019).
- Siddiqui, I. et al. Intratumoral Tcf1⁺PD-1⁺CD8⁺T cells with stem-like properties promote tumor control in response to vaccination and checkpoint blockade immunotherapy. *Immunity* **50**, 195–211.e10 (2019).
- Wherry, E. J. T cell exhaustion. *Nat. Immunol.* **12**, 492–499 (2011).
- Aibar, S. et al. SCENIC: single-cell regulatory network inference and clustering. *Nat. Methods* **14**, 1083–1086 (2017).
- Zander, R. et al. CD4⁺ T cell help is required for the formation of a cytolytic CD8⁺ T cell subset that protects against chronic infection and cancer. *Immunity* **51**, 1028–1042.e4 (2019).
- Dominguez, C. X. et al. The transcription factors ZEB2 and T-bet cooperate to program cytotoxic T cell terminal differentiation in response to LCMV viral infection. *J. Exp. Med.* **212**, 2041–2056 (2015).
- Cedeno-Laurent, F. & Dimitroff, C. J. Galectin-1 research in T cell immunity: past, present and future. *Clin. Immunol.* **142**, 107–116 (2012).

38. Baeyens, A., Fang, V., Chen, C. & Schwab, S. R. Exit strategies: S1P signaling and T cell migration. *Trends Immunol.* **36**, 778–787 (2015).
39. Schiavoni, G., Mattei, F. & Gabriele, L. Type I interferons as stimulators of DC-mediated cross-priming: impact on anti-tumor response. *Front Immunol.* **4**, 483 (2013).
40. Trinchieri, G. Interleukin-12 and the regulation of innate resistance and adaptive immunity. *Nat. Rev. Immunol.* **3**, 133–146 (2003).
41. Kranz, L. M. et al. Systemic RNA delivery to dendritic cells exploits antiviral defence for cancer immunotherapy. *Nature* **534**, 396–401 (2016).
42. Lewis, S. M., Williams, A. & Eisenbarth, S. C. Structure and function of the immune system in the spleen. *Sci. Immunol.* **4**, eaau6085 (2019).
43. Dorner, B. G. et al. Selective expression of the chemokine receptor XCR1 on cross-presenting dendritic cells determines cooperation with CD8⁺ T cells. *Immunity* **31**, 823–833 (2009).
44. Scott, A. C. et al. TOX is a critical regulator of tumour-specific T cell differentiation. *Nature* **571**, 270–274 (2019).
45. Alfei, F. et al. TOX reinforces the phenotype and longevity of exhausted T cells in chronic viral infection. *Nature* **571**, 265–269 (2019).
46. Khan, O. et al. TOX transcriptionally and epigenetically programs CD8⁺ T cell exhaustion. *Nature* **571**, 211–218 (2019).
47. Beltra, J.-C. et al. Developmental relationships of four exhausted CD8⁺ T cell subsets reveals underlying transcriptional and epigenetic landscape control mechanisms. *Immunity* **52**, 825–841.e8 (2020).
48. Hailemichael, Y. et al. Persistent antigen at vaccination sites induces tumor-specific CD8⁺ T cell sequestration, dysfunction and deletion. *Nat. Med.* **19**, 465–472 (2013).
49. Irvine, D. J., Swartz, M. A. & Szeto, G. L. Engineering synthetic vaccines using cues from natural immunity. *Nat. Mater.* **12**, 978–990 (2013).
50. Merad, M., Sathe, P., Helft, J., Miller, J. & Mortha, A. The dendritic cell lineage: ontogeny and function of dendritic cells and their subsets in the steady state and the inflamed setting. *Annu. Rev. Immunol.* **31**, 563–604 (2013).

Publisher's note Springer Nature remains neutral with regard to jurisdictional claims in published maps and institutional affiliations.

This is a U.S. government work and not under copyright protection in the U.S.; foreign copyright protection may apply 2020

Methods

Mice. Female B6 mice (C57Bl/6J), *Ccr2*^{-/-}, *Batf3*^{-/-}, *Ifnar*^{-/-}, *Tlr7*^{-/-} and *Il12b*^{-/-} were purchased from The Jackson Laboratory and maintained in pathogen-free conditions. OT-I Rag2 transgenic mice were purchased from Taconic. *CCR2*^{DTR} mice⁵¹ were bred in-house. Mice were used in studies when 6–8 weeks old. All animal experiments were performed at the Vaccine Research Center at the National Institutes of Health (NIH) with the approval of the Institutional Animal Care and Use Committee at the NIH. Experiments complied with the ethical guidelines set by the Institutional Animal Care and Use Committee and animals were humanely killed at defined end points.

Generation of bone marrow chimeras. Eight-week-old recipient mice received 13 Gy of γ -irradiation (2 doses of 6.5 Gy each) before IV reconstitution with bone marrow from *CCR2*^{DTR} mice. Four to eight weeks after reconstitution, successful chimerism was assessed by flow cytometry. Mice were used in studies eight weeks after reconstitution.

In vivo depletions. For the cell depletion experiments using neutralizing antibodies, mice were injected with 200 μ g per mouse of either anti-CD8 β (clone 53-5.8; Bio X Cell), anti-CD4 (clone GK1.5; Bio X Cell), anti-NK1.1 (clone PK136; Bio X Cell) and the respective isotype controls (Bio X Cell). For the cell depletion experiments in conditional knockout mice (*Ccr2*^{DTR}), 10 ng g⁻¹ body weight of diphtheria toxin were injected intraperitoneally on days −1, 1 and 3 relative to the time of vaccination.

Vaccines. SNP conjugate vaccines were produced as described previously¹¹. Briefly, peptide antigens (GenScript) were linked to hydrophobic blocks containing imidazoquinoline-based TLR7/8a (Aveida Technologies) using a click chemistry reaction. For the pharmacokinetics studies, SNP conjugate vaccines were produced by linking Alexa Fluor 647 to hydrophobic blocks.

Immunizations and treatments. Vaccines were prepared in sterile PBS (Gibco) and administered subcutaneously to each footpad (50 μ l per site) or intravenously via tail vein injection (200 μ l). Animals were treated with 200 μ g per mouse of anti-PD-L1 (10F.9G2; Bio X Cell) in 100 μ l of PBS via intraperitoneal injection.

Cells. The MC38 cell line was a kind gift from L. Delamarre (Genentech). Working cell banks were generated immediately on receipt and used for the tumor experiments. Cells were tested regularly for *Mycoplasma* contamination and none tested positive throughout the studies.

Tumor implantation. MC38 tumor cells were cultured in complete DMEM (Gibco) supplemented with 10% heat-inactivated FCS (Atlanta Biologicals), 100 U ml⁻¹ penicillin, 100 μ g ml⁻¹ streptomycin (Gibco), 1 nonessential amino acids (GE Healthcare Life Sciences) and 1 mM sodium pyruvate (GE Healthcare Life Sciences). For each tumor implantation, a frozen cell aliquot was thawed and cultured in medium at 37 °C and 5% CO₂, passaged once and collected using trypsin EDTA (Gibco). Then, 10⁵ cells in sterile PBS per mouse were implanted subcutaneously on the right flank. Tumors were measured twice a week using digital calipers. Tumor volume was estimated using the formula: (tumor volume = short \times short \times long/2). Animals were killed when tumors reached the size criteria of 1,000 mm³.

Blood and tissue processing. Heparin-treated blood was collected and lysed with ACK lysis buffer (Quality Biological). Lungs, liver, kidneys and tumors were collected in digestion media containing Roswell Park Memorial Institute (RPMI) 1640, 10% FCS, 50 U ml⁻¹ DNase I (Sigma-Aldrich) and 0.2 mg ml⁻¹ collagenase D (Sigma-Aldrich). Tissues were mechanically disrupted using the respective programs on the gentleMACS dissociator (Miltenyi Biotec) and incubated at 37 °C for 30–45 min in a shaking incubator. Spleens were mechanically disrupted and lysed with ACK lysis buffer. Lymph nodes were mechanically disrupted in BioMasher tubes (Nippi). All single-cell suspensions were filtered through a 40- μ m nylon mesh filter plate (Merck Millipore) or 70- μ m cell strainer and resuspended in PBS for flow cytometry staining. For ex vivo cultures, cells were resuspended in RPMI 1640 medium (GE Healthcare Life Sciences) supplemented with 10% heat-inactivated FCS, L-Glutamine–Penicillin–Streptomycin (Sigma-Aldrich), nonessential amino acids, sodium pyruvate (HyClone), HEPES buffer (HyClone) and β -mercaptoethanol (Sigma-Aldrich).

Peptide restimulation. Cells were cultured in vitro with 2 μ g ml⁻¹ Reps1 peptide antigen (GenScript) and 2 μ g ml⁻¹ anti-CD28 (clone 37.51; BD Biosciences) for 6 h. Then, 10 μ g ml⁻¹ of brefeldin A (BD Biosciences) was added in the last 4 h.

Flow cytometry. For T cell tetramer analysis, cells were assessed for viability with LIVE/DEAD Fixable Blue Dead Cell Stain Kit (Invitrogen) in PBS containing 50 nM dasatinib (STEMCELL Technologies) for 30 min at room temperature, washed and blocked with anti-CD16/CD32 (BD Biosciences). Cells were then stained with fluorescently conjugated Reps1 (H-2D^b AQLANDVV) tetramer in cell staining buffer (PBS and 2% FCS) containing dasatinib to enhance staining.

Cells were simultaneously stained with the following surface antibodies to: CD8 (clone 53-6.7), PD-1 (clone 29FA12), CXCR3 (clone 173), CD62L (clone MEL-14), Tim-3 (clone RMT3-23), CD44 (clone IM7), CD39 (clone Duha59), CD127 (clone A7R34) and NKG2A (clone 16A11), purchased from BioLegend and CD4 (clone RM4-4), KLRG1 (clone 2F1) and CD103 (clone M290) purchased from BD Biosciences. After a 1-h incubation at 4 °C, cells were washed twice in cell staining buffer, fixed and permeabilized using the transcription factor staining buffer set (eBioscience). Cells were stained overnight at 4 °C with the following intracellular antibodies to: CD3 (clone 17A2) and Ki-67 (clone Ki-67) from BioLegend, TCF1 (clone C63D9) from Cell Signaling Technology, T-bet (clone O4-46) and granzyme B (clone GB11) from BD Biosciences and EOMES (clone Dan11mag) from Invitrogen.

For the intracellular cytokine analysis after peptide restimulation, cells were assessed for viability with the LIVE/DEAD Fixable Blue Dead Cell Stain Kit (Invitrogen) for 10 min at room temperature. Similar to the antibodies used in the tetramer analysis, cells were blocked with anti-FcR antibodies and stained with cell surface antibodies for 20 min at room temperature in cell staining buffer. Cells were fixed and permeabilized using Fix/Perm solution (BD Biosciences) and subsequently stained with intracellular antibodies to: CD3, IFN- γ (clone XMG1.2), IL-2 (clone JES6-5H4) and TNF (clone MP6-XT22) purchased from BD Biosciences.

For the mononuclear phagocyte uptake analysis, cells were assessed for viability with the LIVE/DEAD Fixable Blue Dead Cell Stain Kit for 10 min at room temperature. After FcR blocking, cells were stained with the following surface antibodies to: NK1.1, CD19 (clone 1D3), CD3 (clone 145-2C11), Ly6G (clone 1A8), CD45 (clone 30-F11), Siglec-H (clone 440c), CD86 (clone GL1), CD11c (clone HL3), CD80 (clone 16-10A1), B220, CD64 (clone X54-5/7.1), CD11b and Ly6C (clone AL-21) purchased from BD Biosciences, CCR7 (clone 4B12), MHC class II (I-A/I-E, clone M5/114.15.2), CD169 (clone 3D6.112) and XCR1 (clone ZET) purchased from BioLegend, and CD172a (clone P84) from Thermo Fisher Scientific.

Cells were acquired on an LSRFortessa X50 (BD Biosciences) using the FACSDiva software v8.0.1 (BD Biosciences) and analyzed on the FlowJo software v10.6.1 (FlowJo LLC).

OT-I in vivo proliferation assay. Spleens and lymph nodes were collected from CD45.2 OT-I mice and labeled with Tag-it Violet Proliferation and Cell Tracking Dye (BioLegend) according to the manufacturer's protocol. Labeled cells (2 \times 10⁶) were transferred via retro-orbital intravenous injection to each congenic CD45.1 mouse at different time points after vaccination. Four days after transfer, spleens were collected from recipient mice for flow cytometry analysis.

In vivo imaging. Whole-body imaging of mice after immunization with Alexa Fluor 647-labeled vaccines was performed using the IVIS Spectrum In Vivo Imaging System (PerkinElmer).

Cell sorting for scRNA-seq. Spleens from mice vaccinated with SNP via SC or IV injections were collected 2 weeks after boost and processed into a single-cell suspension by mechanical dissociation. Splenocytes were stained with Reps1 tetramer and hashtag antibodies (Total-Seq-C antibodies 1–5; BioLegend)⁵². CD8 \pm T cells were isolated by fluorescence-activated cell sorting into 1.5-ml Eppendorf tubes containing staining buffer (2% FCS/PBS). Up to 4 \times 10⁴ cells were sorted per mouse. Cells from mice in both treatment groups with distinct hashtags were mixed to form two pools with an aim for equivalent numbers of cells from each mouse. Each pool of cells was loaded in duplicate into a Chromium single cell sorting system (10x Genomics). Expression and hashtag library construction was performed by following the Chromium Single Cell VDJ Library protocol with a loading target of 1 \times 10⁴ cells per lane. The resulting four libraries were pooled before sequencing on a NovaSeq 6000 S1 chip.

Data processing for scRNA-seq. Raw sequencing files were aligned to the mouse mm10 genome using the Cell Ranger software v3.0.1 (10x Genomics). Hashtag data were added to each expression library using Seurat v.3.1 and demultiplexed using the HTDRemux function. After demultiplexing, singlet cells identified by hashtag from each of the libraries were pooled into a single Seurat object. Cells were further filtered by excluding those with >5% mitochondrial genes in their library and fewer than 1,000 genes¹⁸; 19,368 cells remained after filtering and were used for the downstream analysis.

Downstream analysis of scRNA-seq data. Principal component analysis, UMAP for dimension reduction⁵³, cell clustering (by the Leiden method), constructing a trajectory and pseudotime analyses⁵⁴ were performed on unique molecular identifier counts using Monocle 3 (R package, v.0.2.1) (ref. ⁵⁵). Analysis of DEGs and heatmaps were performed on the log-normalized data with Seurat (R package, v.3.1.4) (ref. ⁵⁶). The differential expression among the clusters was tested using the nonparametric Wilcoxon rank-sum test followed by Bonferroni correction (using all features) to calculate the adjusted P values. Top DEGs were visualized using the SeqGeq software (FlowJo LLC). The SCENIC pipeline (R package, v.1.1.2.2) was used to construct and score gene regulatory networks (regulons) as described

previously³⁴. Each regulon is composed of a transcription factor and its putative target genes. The output of SCENIC is a matrix of the activity of regulons, where rows correspond to regulons and columns correspond to cells.

TCR analysis of scRNA-seq data. TCR libraries were generated independently for all four 10x lanes according to the Chromium Single Cell VDJ Library protocol. Raw sequencing files were aligned to the mouse mm10 genome and annotated with their TCR genes by using the cellranger vdj function from the Cell Ranger software suite (10x Genomics). We excluded cells that did not have full-length or productive TCR- α (*TRA*) or TCR- β (*TRB*) gene pairs and those with multiple gene pairs (duplicates). Filtered *TRA/TRB* gene pairs were matched to the cells used for the gene expression analysis by 10x barcode and any *TRA/TRB* pair that was not present in our gene expression dataset was removed from further analysis. Clonotype was assigned based on the complementarity-determining region 3 amino acid sequence of the *TRA/TRB* gene pair. Only clonotypes expressed by more than 100 cells were visualized in the heatmap.

ELISA. Serum from whole blood, spleens and popliteal lymph nodes was collected at specified time points after vaccination. Supernatants were collected from single-cell suspensions of spleens and lymph nodes that were cultured *in vitro* for 12 h in complete RPMI 1640 at 37 °C. Commercially available ELISA kits were used to measure IL-12 subunit p40 (PeproTech) and all subtypes of IFN- α (PBL Assay Science) according to the manufacturer's protocols.

Confocal microscopy. Spleens and popliteal lymph nodes were collected at the indicated times and prepared as described previously⁵⁷. Briefly, tissues were fixed in periodate-lysine-parafomaldehyde buffer and placed in 30% sucrose in PBS. Tissues were then embedded in optimal cutting temperature medium (Electron Microscopy Sciences), frozen in dry ice-cooled isopentane and sections were cut on a cryostat (Leica Microsystems). Sections were blocked in 5% sera and stained with the following antibodies to: CD11b (clone M1/70; eBioscience), CD11c (clone N418; eBioscience), B220 (clone RA3-6B2; eBioscience), CD64 (polyclonal; R&D Systems), MHC complex II, followed by the relevant secondary antibodies conjugated to fluorophores. Images were acquired using a Leica SP8 microscope and analyzed with the Imaris software v9.5.0 (Bitplane).

Statistical analysis. All results are presented as the median with s.d. Statistics were assessed using a Kruskal–Wallis test with Dunn's correction for multiple comparisons, two-way analysis of variance (ANOVA) with Bonferroni correction, log-rank test and Mann–Whitney *U*-test for immunogenicity (Prism; GraphPad Software v8.4.2).

Reporting Summary. Further information on research design is available in the Nature Research Reporting Summary linked to this article.

Data availability

The data that support the findings of this study are available from the corresponding author upon request. The scRNA-seq data have been uploaded to the Gene Expression Omnibus (accession number [GSE158240](#)).

References

51. Hohl, T. M. et al. Inflammatory monocytes facilitate adaptive CD4 T cell responses during respiratory fungal infection. *Cell Host Microbe* **6**, 470–481 (2009).

52. Stoeckius, M. et al. Cell Hashing with barcoded antibodies enables multiplexing and doublet detection for single cell genomics. *Genome Biol.* **19**, 224 (2018).
53. Becht, E. et al. Dimensionality reduction for visualizing single-cell data using UMAP. *Nat. Biotechnol.* **37**, 38–44 (2019).
54. Saelens, W., Cannoodt, R., Todorov, H. & Saeys, Y. A comparison of single-cell trajectory inference methods. *Nat. Biotechnol.* **37**, 547–554 (2019).
55. Trapnell, C. et al. The dynamics and regulators of cell fate decisions are revealed by pseudotemporal ordering of single cells. *Nat. Biotechnol.* **32**, 381–386 (2014).
56. Butler, A., Hoffman, P., Smibert, P., Papalexi, E. & Satija, R. Integrating single-cell transcriptomic data across different conditions, technologies, and species. *Nat. Biotechnol.* **36**, 411–420 (2018).
57. Reynoso, G. V. et al. Lymph node conduits transport virions for rapid T cell activation. *Nat. Immunol.* **20**, 602–612 (2019).

Acknowledgements

We thank members of the Seder lab for scientific discussions; S. Darko, A. Ransier and D. Douek for scRNA-seq advice; and M. Dillon, G. Salvador, S. Rush, L. Gilliam, O. Hernandez, C. Chiedi and D. Scorpio of the Translational Research Program (Vaccine Research Center) for their valuable support with the animal studies. This work was supported by the Intramural Research Program of the U.S. NIH (R.A.S., H.D.H. and J.S.T.), EMBO YIP and Singapore Immunology Network core funding (F.G.).

Author contributions

F.B., A.S.I. and R.A.S. conceived and designed the experiments. F.B., R.A.R.-V., K.K.S.T. and H.Y. performed the experiments including animal work, flow cytometry and ELISA. R.A.R.-V., C.-A.D. and A.K. performed the scRNA-seq data analysis with the support of M.P.M., A.J.M., J.S.T., X.M.Z. and F.G. F.B., G.V.R. and H.D.H. performed and analyzed the confocal microscopy data. J.A.H., J.P.F. and N.B. provided the mice and reagents for the experiments. G.M.L., V.L.C. and A.S.I. designed and prepared the vaccines for the experiments. F.B. and R.A.S. prepared the figures and wrote the manuscript with input from all authors.

Competing interests

G.M.L., V.L.C., A.S.I. and R.A.S. are listed as inventors on patents describing polymer-based vaccines. G.M.L., V.L.C. and A.S.I. are employees of Avidae Technologies, which is commercializing polymer-based drug delivery technologies for immunotherapeutic applications.

Additional information

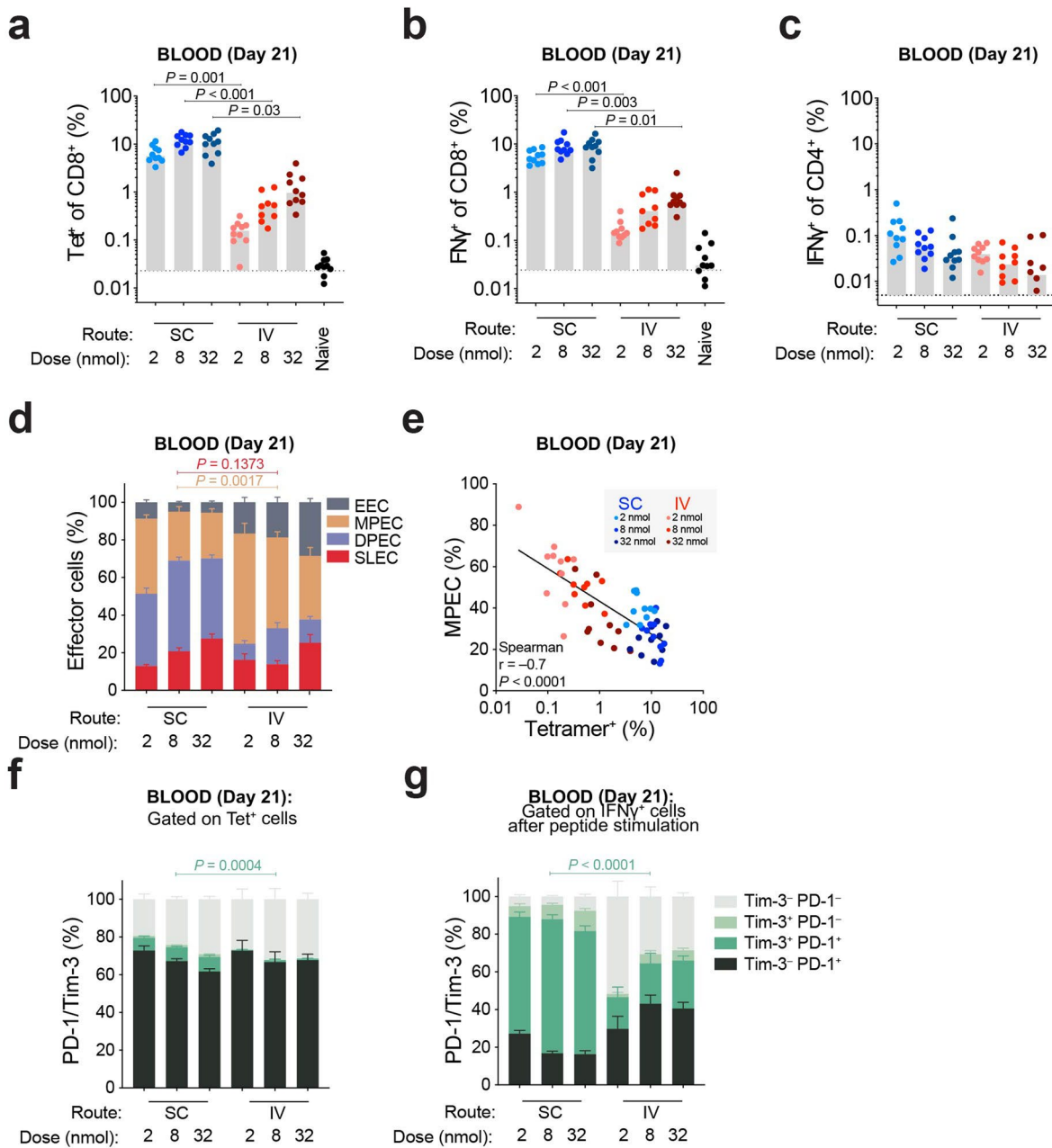
Extended data is available for this paper at <https://doi.org/10.1038/s41590-020-00810-3>.

Supplementary information is available for this paper at <https://doi.org/10.1038/s41590-020-00810-3>.

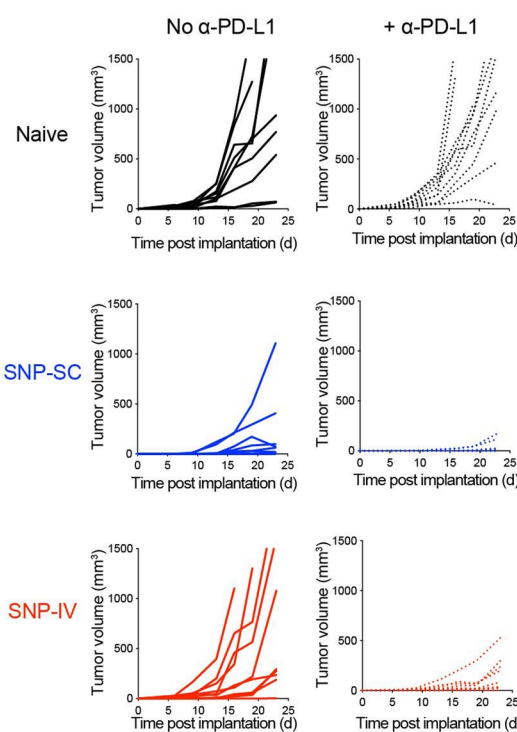
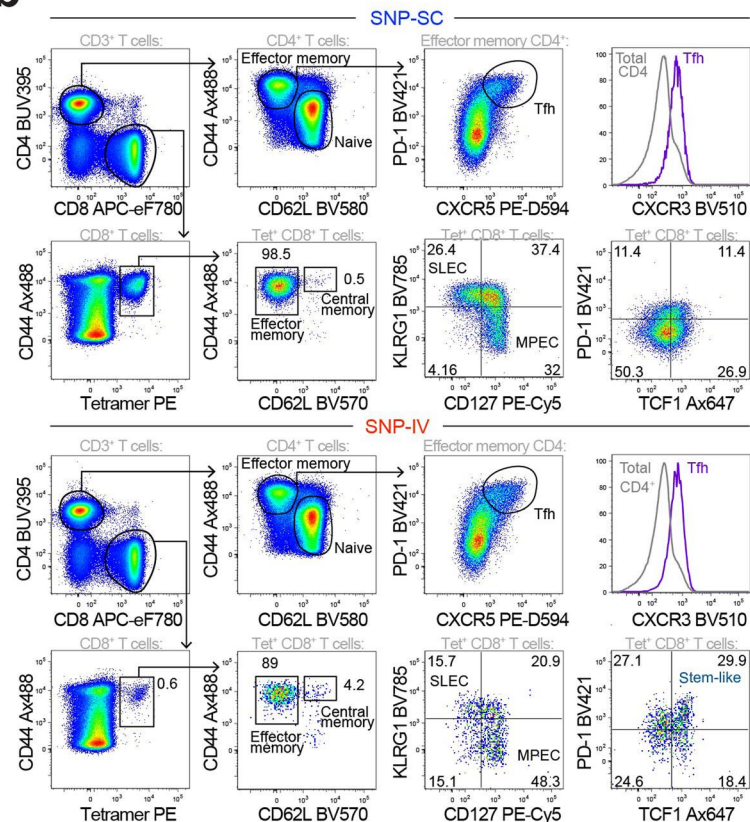
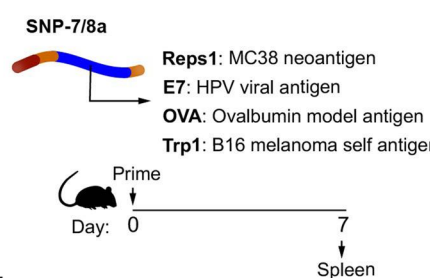
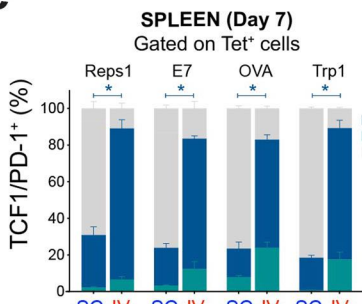
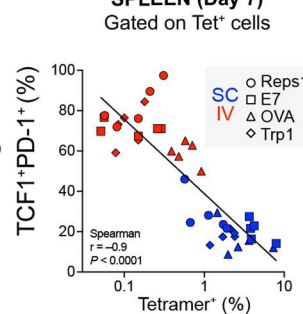
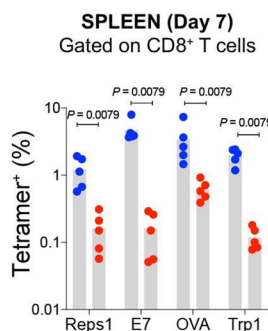
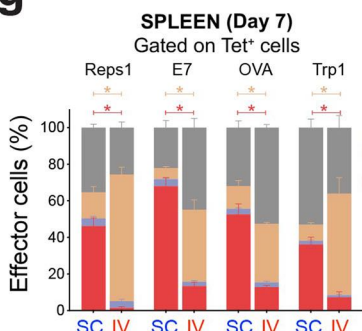
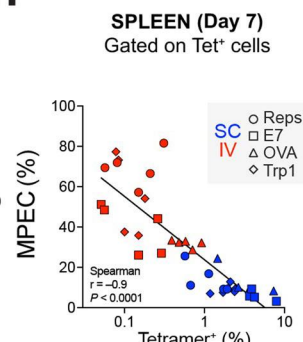
Correspondence and requests for materials should be addressed to R.A.S.

Peer review information Zoltan Fehervari was the primary editor on this article and managed its editorial process and peer review in collaboration with the rest of the editorial team

Reprints and permissions information is available at www.nature.com/reprints.

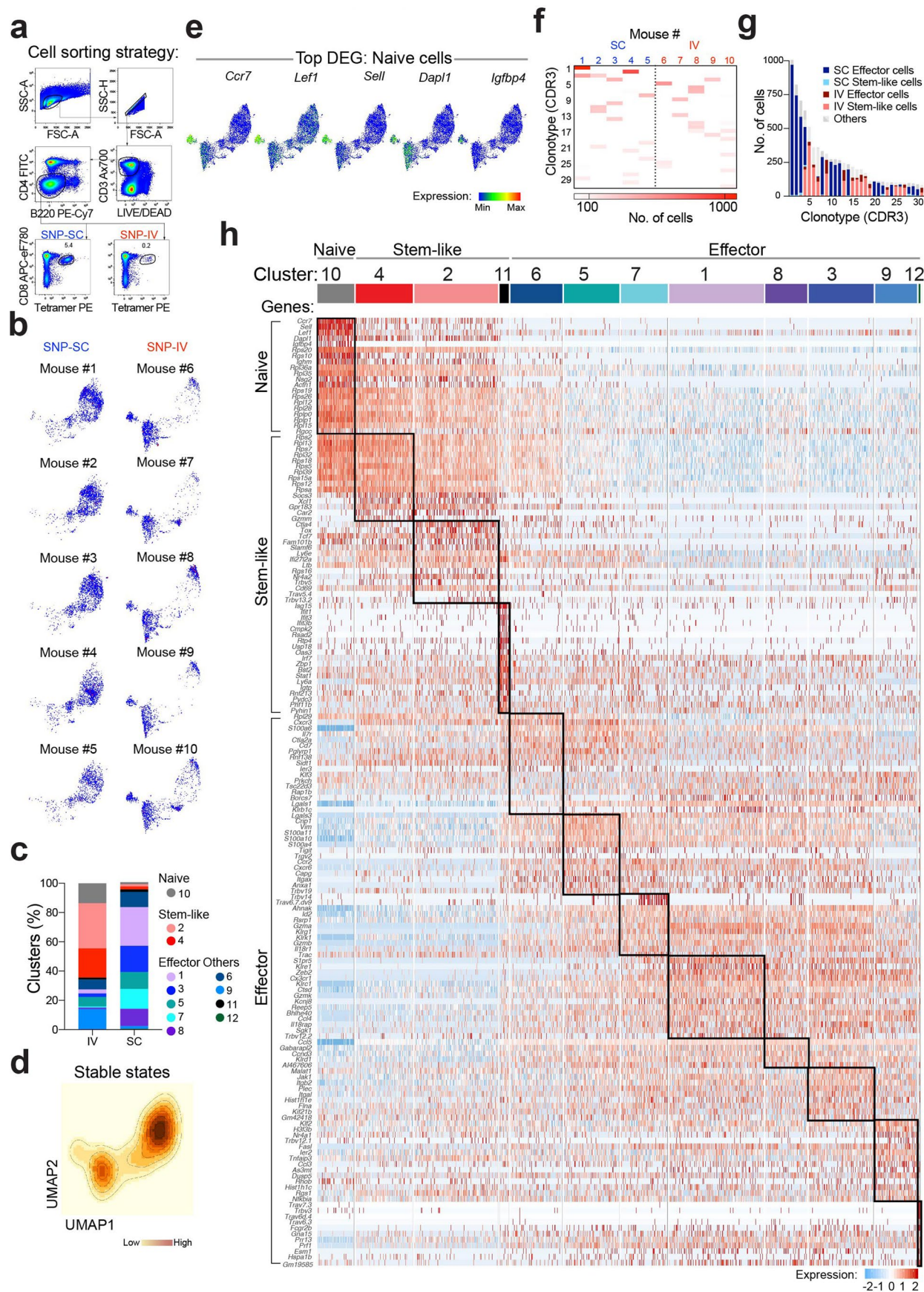


Extended Data Fig. 1 | Route and dose of SNP-7/8a immunization controls the magnitude and phenotype of antigen-specific CD8⁺ T cells. **a**, Whole blood was collected on day 21 to measure the frequency of tetramer⁺ CD8⁺ T cells post boost. Bar graphs summarize the frequency of tetramer⁺ CD8⁺ T cells from blood ($n=10$). **b**, Bar graphs summarize the frequency of IFN γ ⁺ CD8⁺ T cells from blood ($n=10$) on day 21. **c**, Bar graphs summarize the frequency of IFN γ ⁺ CD4⁺ T cells from blood ($n=10$). **d**, Bar graphs show proportions of MPEC/SLEC subpopulations in the blood ($n=10$). **e**, Frequency of MPECs is negatively correlated to frequency of tetramer⁺ CD8⁺ T cells. **f**, **g**, Bar graphs show proportions of PD-1/Tim-3 subpopulations in the blood ($n=10$) of tetramer⁺ cells (**f**) or IFN γ ⁺ cells (**g**). Data are representative of two independent experiments. The bars represent the median (**a–c**) or mean \pm s.e.m. (**d, f, g**). Statistics were assessed by Kruskal-Wallis with Dunn's correction for multiple comparisons (**a, b, d, f, g**) and Spearman correlation (**e**).

a**b****c****e****f****d****g****h**

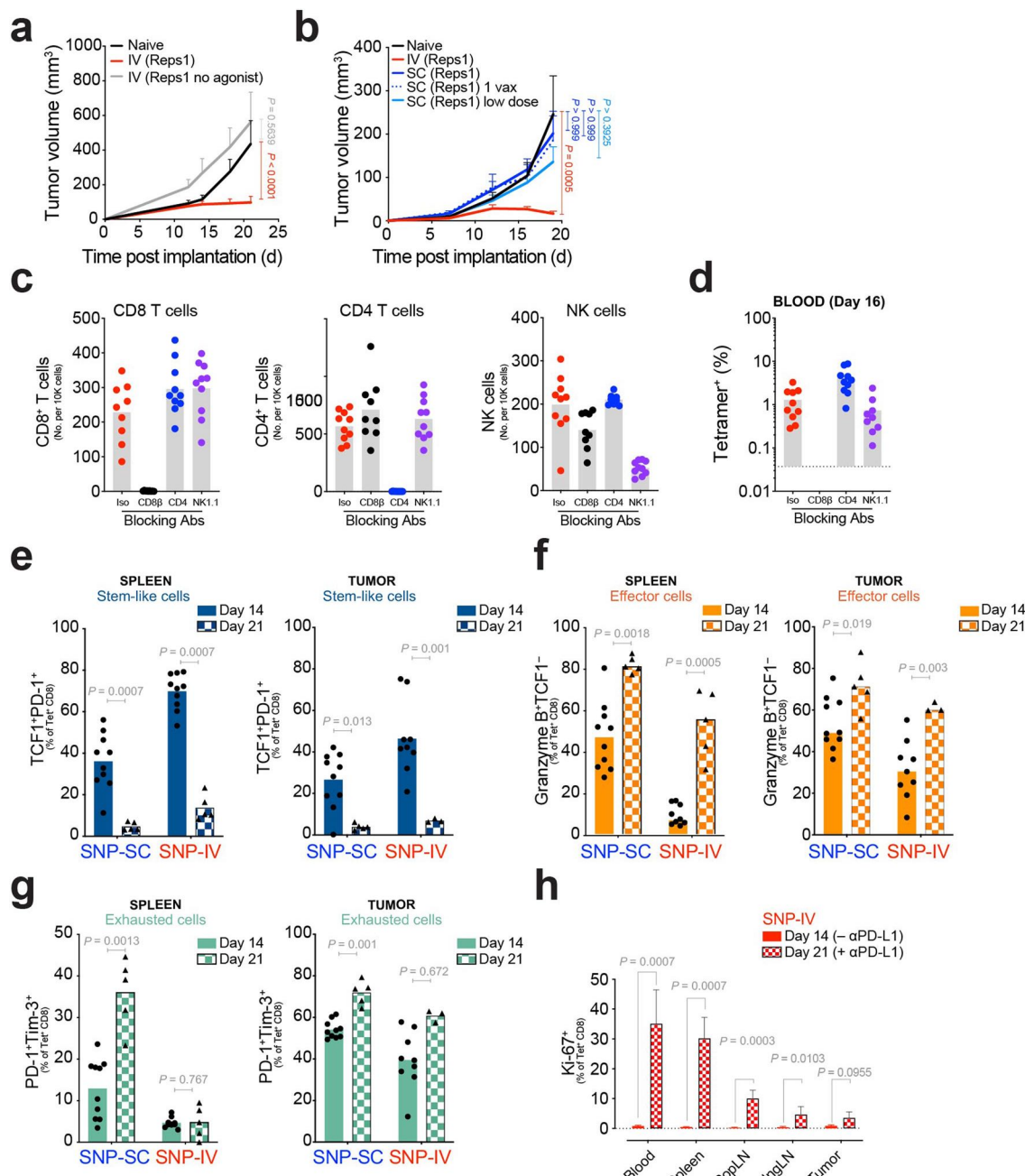
Extended Data Fig. 2 | See next page for caption.

Extended Data Fig. 2 | Intravenous administration of SNP-7/8a generates TCF1⁺ CD8⁺ T cells with anti-tumor capacity upon anti-PD-L1 treatment. **a**, Tumor growth curves of mice unvaccinated (black) or vaccinated with SNP-SC (blue) or SNP-IV (red) with (dotted line) or without α -PD-L1 (solid line) ($n=10$). **b**, Flow cytometric analysis of single cells from spleen (concatenated, $n=6$) after SNP-SC (top panel) or SNP-IV (bottom panel). Cells were stained with Reps1 tetramer and other antibodies. Numbers indicate percentage of cell population within the gate. **c**, Mice were vaccinated with SNP-7/8a containing Reps1, E7, OVA or Trp1 antigens ($n=5$). Spleens were collected 7 days post prime. **d**, Splenocytes were stained with tetramers specific for the respective antigens. Bar graph summarizes the frequencies of antigen-specific CD8⁺ T cells following SNP-SC (blue) or SNP-IV (red) ($n=5$). **e**, Bar graph summarizes the frequencies of TCF1 subpopulations in the spleen ($n=5$) after SNP-SC or SNP-IV. **f**, Frequency of TCF1⁺PD-1⁺ cells is negatively correlated to frequency of tetramer⁺ CD8⁺ T cells. **g**, Bar graph summarizes the frequencies of early effector cells (EEC, gray), memory precursor effector cells (MPEC, tan), double positive effector cells (DPEC, lilac) and short lived effector cells (SLEC, crimson) in the spleen ($n=5$) after SNP-SC or SNP-IV. **h**, Frequency of MPEC is negatively correlated to frequency of tetramer⁺ CD8⁺ T cells. The bars represent mean \pm s.e.m. (**d,e,g**). Statistics were assessed by Mann Whitney test (**d, e, g**) and Spearman correlation (**f, h**).

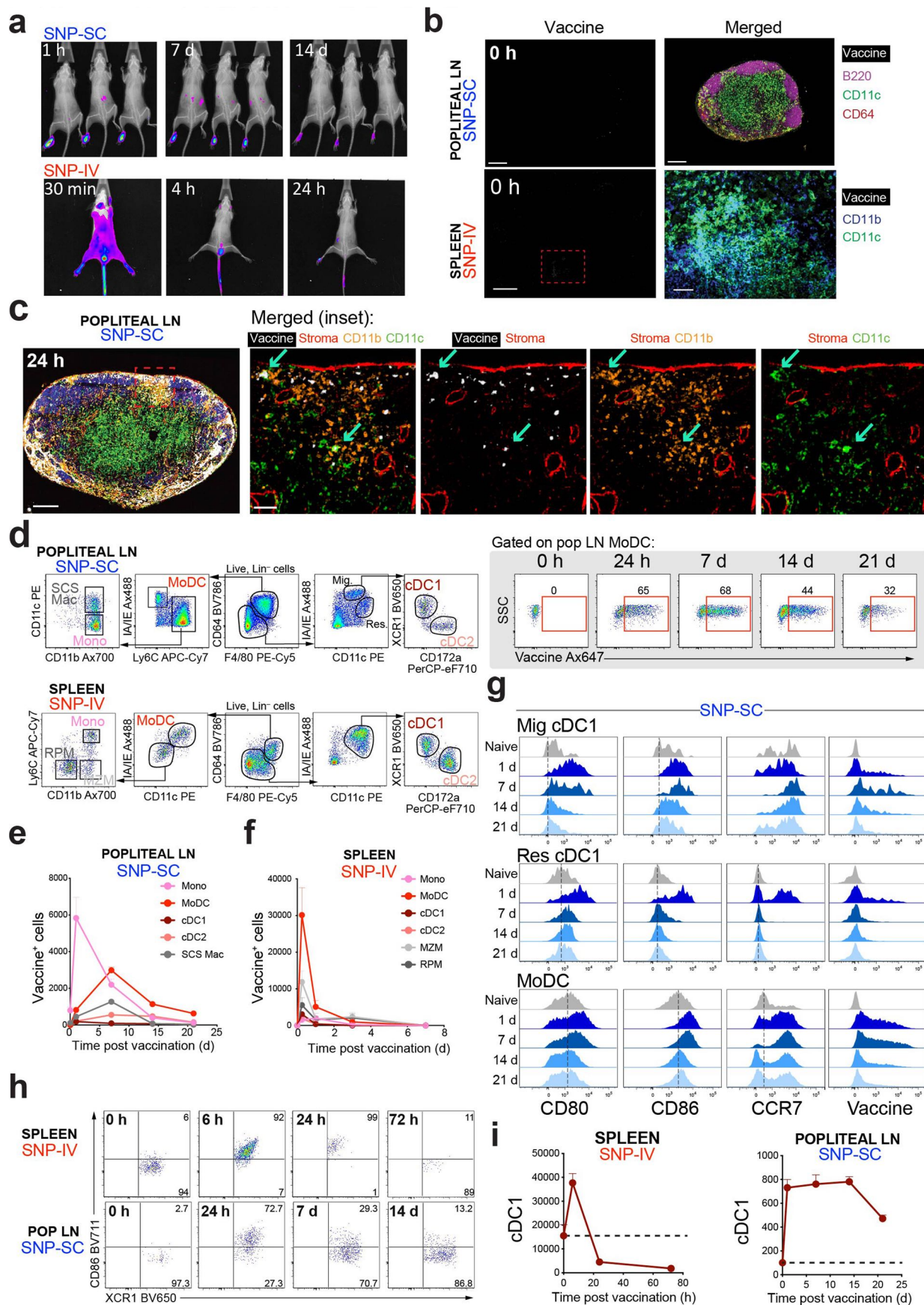


Extended Data Fig. 3 | See next page for caption.

Extended Data Fig. 3 | Single-cell analysis of neoAg⁺ CD8⁺ T cells by RNA sequencing identifies stem-like gene signature in SNP-IV and effector gene signature in SNP-SC cells. **a**, C57BL/6 mice ($n=5$) were vaccinated subcutaneously or intravenously at 8 nmol on day 0 and day 14 with SNP-7/8a containing Reps1. Spleens were collected on day 28 and tetramer⁺ CD8⁺ T cells were sorted by flow cytometry. Flow plots show gating strategy for cell sorting. **b**, Mice were individually labeled with distinct hashtag oligo-tagged antibodies and pooled for 10x and RNA sequencing. Individual UMAPs show gene expression of each mouse vaccinated SC (left panel) or IV (right panel). **c**, Bar graph summarizes the frequency of the twelve Monocle 3 clusters that are represented by each vaccination route ($n=5$). **d**, Density plots to identify stability states corresponding to higher density areas on UMAP, based on 2D kernel density estimation. **e**, Expression of top differentially expressed genes (DEG) of naïve cells are presented in meaning plots. **f**, Heatmap summarizes the number of cells that share a clonotype based on paired alpha and beta complementarity-determining region 3 (CDR3) sequences in each individual animal. **g**, Bar graph shows numbers of stem-like cells (clusters 2 and 4) and effector cells (clusters 1, 3, 5, 7 and 8) in each clonotype from SC or IV vaccinated mice. Only clonotypes expressed by more than 100 cells are represented in the graphs. **h**, Heatmap of DEG expressed in each cluster organized along the pseudotime trajectory.

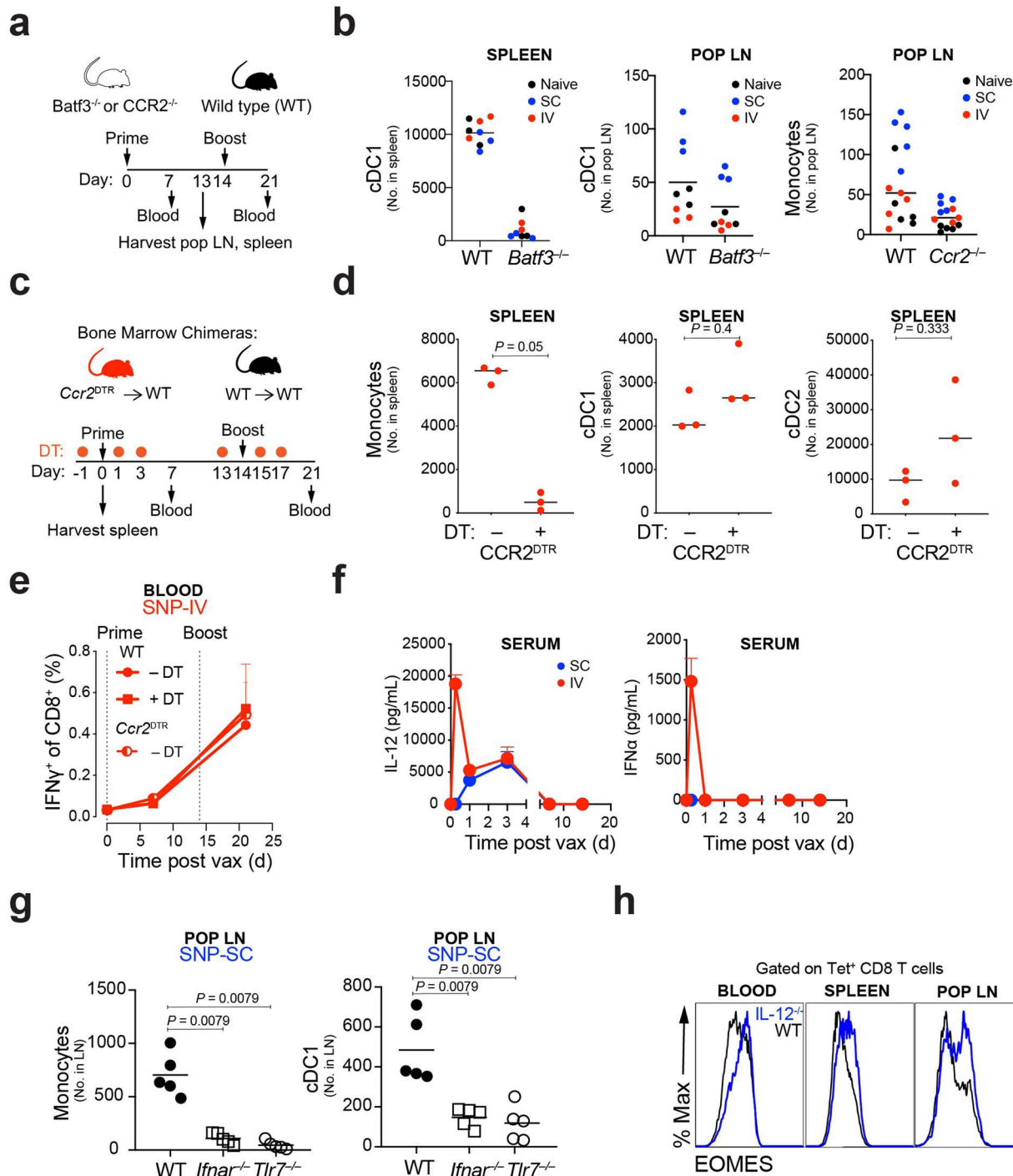


Extended Data Fig. 4 | Therapeutic vaccination with SNP-IV generates neoAg-specific CD8⁺ T cells with superior anti-tumor capacity. **a**, Tumor growth of mice treated with SNP-7/8a with (red) or without agonist (gray) ($n=10$). **b**, Average tumor growth of SNP-IV (red), SNP-SC given twice (blue), once on day 7 (dotted blue) or twice at a lower dose (light blue) ($n=10$). **c**, Total numbers of CD8⁺ T cells, CD4⁺ T cells and NK cells and **d**, frequency of tetramer⁺ CD8⁺ T cells from blood in mice treated with isotype control antibody (red) or blocking antibodies against CD8 β (black), CD4 (blue) or NK1.1 (purple) as assessed by flow cytometry ($n=10$). **e-h**, Spleens and tumors were harvested on day 14 ($n=10$) and day 21 (spleen, $n=5$; tumor, $n=3$). **e**, Stem-like cells (TCF1⁺PD-1⁺; dark blue), **f**, effector cells (Granzyme B⁺TCF1⁻; orange) or **g**, exhausted cells (PD-1⁺Tim-3⁺) of tetramer⁺ cells were identified by flow cytometry. Bar graphs summarize the frequency of cells in the spleen and tumors on day 14 (filled bar) or day 21 (checkered bar). **h**, Bar graphs summarize the frequency of Ki-67⁺ cells in different tissues on day 14 (red bar) or day 21 (checkered bar) post SNP-IV. Data are representative of four independent experiments. Mean \pm s.e.m. Statistics were assessed by two-way ANOVA with Bonferroni correction (**a**, **b**) and Mann Whitney test (**e-h**).



Extended Data Fig. 5 | See next page for caption.

Extended Data Fig. 5 | Transient vaccine distribution to spleen and activation of migratory cDC1 and moDC in after SNP-IV. **a**, Whole body images of mice following SNP-SC or SNP-IV with labeled vaccines. **b**, Confocal images of LN or spleen sections of an unvaccinated mouse. **c**, Confocal image of popliteal LN section post SNP-SC. Detailed overlay of additional markers. White, vaccine; red, ERTR7 (stroma); orange, CD11b (monocytes, macrophages or cDC2); CD11c (moDC or cDC). Scale bar, 200 μ m or 50 μ m (inset). Arrows show co-localization of vaccine and CD11b $^{+}$ CD11c $^{+}$ cells. **d**, Gating strategy to identify various populations from popliteal LN and spleen after SNP-SC and SNP-IV: MoDC (red), monocytes (pink), subcapsular sinus macrophages, SCS (gray), red pulp macrophages, RPM (dark gray), cDC1 (maroon), cDC2 (coral). Kinetics of MNPs that are vaccine $^{+}$ in **e**, popliteal LNs or **f**, spleens after SNP-SC or SNP-IV respectively ($n=3$). **g**, Histograms show MFI of CD80, CD86, CCR7 and labeled vaccine in migratory or resident cDC1 or moDC in popliteal LN of naïve (gray) or SNP-SC mice after vaccination (concatenated, $n=3$). **h**, **i**, Flow cytometric analysis of single cells stained with XCR1 and CD86 after gating on cDC1s in spleens or popliteal LNs of mice post SNP-IV or SNP-SC respectively ($n=3$). Mean \pm s.e.m. (**i**). Data are representative of two independent experiments.



Extended Data Fig. 6 | Prolonged antigen presentation by DC drives CD8⁺ T cell responses after SNP-SC. **a**, WT, *Batf3*^{-/-} or *Ccr2*^{-/-} mice ($n=10$) were vaccinated SC or IV at 8 nmol on day 0 and day 14 with SNP-7/8a (Reps1). **b**, Total number of cDC1 in spleen and popliteal LN, or monocytes in popliteal LN (right panel) of WT, *Batf3*^{-/-} or *Ccr2*^{-/-} were measured ($n=3$). **c**, Bone marrow (BM) chimeras were performed by irradiating WT CD45.1 mice and transferring BM from *Ccr2*^{DTR} or WT CD45.2 mice. After 8 weeks of reconstitution, mice were treated with DT ($n=3$). **d**, Total number of monocytes, cDC1 and cDC2 in spleen of *Ccr2*^{DTR} mice 24 h after DT treatment was measured ($n=3$). **e**, Kinetics of neoAg-specific CD8⁺ T cell responses after SNP-IV in blood of *Ccr2*^{DTR} without DT treatment, or WT CD45.2 BM chimera with or without prior DT treatment showed similar responses ($n=5$). **f**, Sera were collected after SNP-SC (blue) or SNP-IV (red). IL-12 (left panel) or IFN- α (right panel) were measured by ELISA ($n=3$). **g**, Total number of monocytes and cDC1 in popliteal LN of WT, *Ifnar*^{-/-} or *Tlr7*^{-/-} were measured by flow cytometry. **h**, Histograms of EOMES gated on tetramer⁺ cells post SNP-SC in WT or *IL12b*^{-/-} mice ($n=4$). Mean \pm s.e.m. **(e-g)**. Data are representative of two independent experiments. Statistics were assessed by Mann Whitney test **(d)** or Kruskal-Wallis with Dunn's correction for multiple comparisons **(g)**.

Reporting Summary

Nature Research wishes to improve the reproducibility of the work that we publish. This form provides structure for consistency and transparency in reporting. For further information on Nature Research policies, see our [Editorial Policies](#) and the [Editorial Policy Checklist](#).

Statistics

For all statistical analyses, confirm that the following items are present in the figure legend, table legend, main text, or Methods section.

n/a Confirmed

- The exact sample size (n) for each experimental group/condition, given as a discrete number and unit of measurement
- A statement on whether measurements were taken from distinct samples or whether the same sample was measured repeatedly
- The statistical test(s) used AND whether they are one- or two-sided
Only common tests should be described solely by name; describe more complex techniques in the Methods section.
- A description of all covariates tested
- A description of any assumptions or corrections, such as tests of normality and adjustment for multiple comparisons
- A full description of the statistical parameters including central tendency (e.g. means) or other basic estimates (e.g. regression coefficient) AND variation (e.g. standard deviation) or associated estimates of uncertainty (e.g. confidence intervals)
- For null hypothesis testing, the test statistic (e.g. F , t , r) with confidence intervals, effect sizes, degrees of freedom and P value noted
Give P values as exact values whenever suitable.
- For Bayesian analysis, information on the choice of priors and Markov chain Monte Carlo settings
- For hierarchical and complex designs, identification of the appropriate level for tests and full reporting of outcomes
- Estimates of effect sizes (e.g. Cohen's d , Pearson's r), indicating how they were calculated

Our web collection on [statistics for biologists](#) contains articles on many of the points above.

Software and code

Policy information about [availability of computer code](#)

Data collection FACSDiva software v8.0.1 (Flow Cytometry, BD), Leica Application Suite X (Confocal, Leica), Living Image Software v4.7.2 (IVIS imaging, Perkin Elmer).

Data analysis FlowJo v10.6.1 (BD), Prism v8.4.2 (Graphpad), Imaris v9.5.0 (Bitplane), Cell Ranger (10X Genomics), Seurat v3.0 (<https://github.com/satijalab/seurat>), Monocle 3 (<https://github.com/cole-trapnell-lab/monocle3>), SCENIC (<https://github.com/aertslab/SCENIC>)

For manuscripts utilizing custom algorithms or software that are central to the research but not yet described in published literature, software must be made available to editors and reviewers. We strongly encourage code deposition in a community repository (e.g. GitHub). See the Nature Research [guidelines for submitting code & software](#) for further information.

Data

Policy information about [availability of data](#)

All manuscripts must include a [data availability statement](#). This statement should provide the following information, where applicable:

- Accession codes, unique identifiers, or web links for publicly available datasets
- A list of figures that have associated raw data
- A description of any restrictions on data availability

The data that support the findings of this study are available from the corresponding author upon reasonable request. scRNA-seq data is available on GEO (ascension #). Published data sets referred to in Figure 3f are publicly available on GEO: Siddiqui et al (GSE114631), Miller et al (GSE122713), Chen et al (GSE131535)

Field-specific reporting

Please select the one below that is the best fit for your research. If you are not sure, read the appropriate sections before making your selection.

Life sciences

Behavioural & social sciences

Ecological, evolutionary & environmental sciences

For a reference copy of the document with all sections, see nature.com/documents/nr-reporting-summary-flat.pdf

Life sciences study design

All studies must disclose on these points even when the disclosure is negative.

Sample size	No statistical methods were used to predetermine sample size. We follow standards in the field when choosing the sample size, especially with tumor-bearing animals (Yadav et al <i>Nature</i> 2016, Kreiter et al <i>Nature</i> 2016, Lynn et al <i>Nat Biotech</i> 2020)
Data exclusions	For scRNA-seq data, we excluded cells with low number of detected transcripts and high mitochondria content as a pre-established criteria based on other published data (Chen et al <i>Immunity</i> 2019)
Replication	All mouse experiments were successfully replicated in two or more individual cohorts.
Randomization	Animals were randomly assigned to either control or experimental groups.
Blinding	Tumor measurements were performed blinded by de-identifying animals.

Reporting for specific materials, systems and methods

We require information from authors about some types of materials, experimental systems and methods used in many studies. Here, indicate whether each material, system or method listed is relevant to your study. If you are not sure if a list item applies to your research, read the appropriate section before selecting a response.

Materials & experimental systems		Methods	
n/a	Involved in the study	n/a	Involved in the study
<input type="checkbox"/>	<input checked="" type="checkbox"/> Antibodies	<input checked="" type="checkbox"/>	<input type="checkbox"/> ChIP-seq
<input type="checkbox"/>	<input checked="" type="checkbox"/> Eukaryotic cell lines	<input type="checkbox"/>	<input checked="" type="checkbox"/> Flow cytometry
<input checked="" type="checkbox"/>	<input type="checkbox"/> Palaeontology and archaeology	<input checked="" type="checkbox"/>	<input type="checkbox"/> MRI-based neuroimaging
<input type="checkbox"/>	<input checked="" type="checkbox"/> Animals and other organisms		
<input checked="" type="checkbox"/>	<input type="checkbox"/> Human research participants		
<input checked="" type="checkbox"/>	<input type="checkbox"/> Clinical data		
<input checked="" type="checkbox"/>	<input type="checkbox"/> Dual use research of concern		

Antibodies

Antibodies used

T CELL PANEL

CD8 (53-6.7, Biolegend)
 PD-1 (29F.A12, Biolegend)
 CXCR3 (173, Biolegend)
 CD62L (Mel-14, Biolegend)
 Tim-3 (RMT3-23, Biolegend)
 CD44 (IM7, Biolegend)
 CD39 (Duha59, Biolegend)
 CD127 (A7R34, Biolegend)
 NKG2A (16A11, Biolegend)
 CD4 (RM4-4, BD)
 KLRG1 (2F1, BD)
 CD103 (M290, BD)
 CD3 (17A2, Biolegend)
 Ki-67 (Ki-67, Biolegend)
 TCF1 (C63D9, Cell Signaling)
 T-bet (O4-46, BD)
 Granzyme B (GB11, BD)
 Eomes (Dan11mag, Invitrogen)
 IFN-γ (XMG1.2, BD)
 IL-2 (JES6-5H4, BD)
 TNF (MP6-XT22, BD)

LIVE/DEAD Fixable Blue (Invitrogen)

MNP PANEL

NK1.1 (PK136, BD)
 CD19 (1D3, BD)
 CD3 (145-2C11, BD)
 Ly6G (1A8, BD)
 CD45 (30-F11, BD)
 SiglecH (440c, BD)
 CD86 (GL1, BD)
 CD11c (HL3, BD)
 CD80 (16-10A1, BD)
 B220 (RA3-6B2, BD)
 CD64 (X54-5/7.1, BD)
 CD11b (MI/70, BD)
 Ly6C (AL-21, BD)
 CCR7 (4B12, Biolegend)
 MHCII (I-A/I-E, M5/114.15.2, Biolegend)
 CD169 (3D6.112, Biolegend)
 XCR1 (ZET, Biolegend)
 CD172a (P84, Life Technologies)

Validation

All antibodies were commercially available and titrated on relevant cells prior to usage.

Eukaryotic cell linesPolicy information about [cell lines](#)

Cell line source(s)

MC38 was a kind gift from Lélia Delamarre (Genentech, USA).

Authentication

Cell lines were used without further authentication.

Mycoplasma contamination

MC38 was tested for mycoplasma prior to tumor implantation studies and confirmed to be negative.

Commonly misidentified lines
(See [ICLAC](#) register)

No commonly misidentified lines were used in this study.

Animals and other organismsPolicy information about [studies involving animals; ARRIVE guidelines](#) recommended for reporting animal research

Laboratory animals

Mice (Mus musculus, strain C57BL/6, female, age 6–8 weeks, Jackson laboratories). Specific strains of knockouts are listed in the online methods.

Wild animals

The study did not involve wild animals.

Field-collected samples

The study did not involve field-collected samples.

Ethics oversight

All animal studies complied with ethical guidelines set by Institutional Animal Care and Use Committee (ACUC) at the National Institutes of Health (NIH, USA). Animals were humanely euthanized at defined endpoints.

Note that full information on the approval of the study protocol must also be provided in the manuscript.

Flow Cytometry**Plots**

Confirm that:

- The axis labels state the marker and fluorochrome used (e.g. CD4-FITC).
- The axis scales are clearly visible. Include numbers along axes only for bottom left plot of group (a 'group' is an analysis of identical markers).
- All plots are contour plots with outliers or pseudocolor plots.
- A numerical value for number of cells or percentage (with statistics) is provided.

Methodology

Sample preparation

Single cell suspension was generated from mouse blood, spleens, lymph nodes, lungs, livers, kidneys and tumors. Spleens and lymph nodes were processed by mechanical disruption, whereas all other tissues were enzymatically digested with Collagenase and DNase as described in the online methods. Cells were filtered and treated with red blood cell lysis buffer.

Instrument	Modified LSRFortessa X-50 (BD)
Software	FACSDiva software v8.0.1, FlowJo v10.6.1 (BD)
Cell population abundance	Relevant cell population abundance is noted in each figure.
Gating strategy	<p>All analyses begin with singlet (FSC-A vs FSC-H) > Leukocyte (FSC-A vs SSC-A) > Live cells.</p> <p>For T cell analyses, cells were gated on CD3 and then CD4 or CD8. For peptide re-stimulation assays, cells were gated on IFN-gamma. For tetramer analysis, cells were gated on CD44 vs tetramer. Downstream phenotypic analysis are based on tetramer+ CD8 T cells. All gates were set based on total CD8 T cells for clear positive and negative populations.</p> <p>For mononuclear phagocyte analysis, lineage cells were excluded (Ly6G+, SSChi, NK1.1+, CD19+, CD3+). Monocytes and macrophages were gated based on expression of CD64 or F4/80. Monocyte-derived dendritic cells (moDC) were identified by MHCI+ CD11c+. Monocytes were identified as Ly6C+ of the non-MoDC. Conventional dendritic cells (DC) were identified based on non-monocyte/macrophages that were MHCI+ CD11c+, followed by XCR1+ (cDC1) or CD172a+ (cDC2). Downstream expression of labeled vaccine or activation markers are based on identified populations.</p>

Tick this box to confirm that a figure exemplifying the gating strategy is provided in the Supplementary Information.